博士論文

Development of a novel miR-34-regulated oncolytic coxsackievirus B3 with minimal toxicity and strong anti-tumor activity.

（低臓器障害性で強力な抗腫瘍活性を有する miR-34 制御新規腫瘍溶解性コクサッキーウイルス B3 の開発）

か　よう

賈　楊

Jia Yang

Development of a novel miR-34-regulated oncolytic coxsackievirus B3 with minimal toxicity and strong anti-tumor activity.

（低臓器障害性で強力な抗腫瘍活性を有する miR-34 制御新規腫瘍溶解性コクサッキーウイルス B3 の開発）

東京大学　医学系研究科　内科学専攻

ALA 先端医療学社会連携研究部門

指導教員　谷　憲三朗

Jia Yang

賈　楊

Abstract

Oncolytic virotherapies have emerged as new modalities for cancer treatment. Our lab previously reported that coxsackievirus B3 (CVB3) is a novel oncolytic virus (OV) with a strong ability to lyse human non–small cell lung cancer cells; however, its non-specific toxicity against normal cells remains to be resolved (*1*). To improve its safety profile, microRNA target sequences complementary to miR-34a/c, which is expressed preferentially in normal cells, were inserted into the 5'UTR or 3'UTR of the CVB3 genome. In the presence of miR-34a/c, the gene-modified CVB3 could not replicate in normal cells. We also found that the pathogenicity of CVB3 was reduced to greater extent by targeting miR-34a than miR-34c; in addition, it was more effective to insert the target sequences into the 3'UTR rather than the 5'UTR of the viral genome. Ultimately, we developed a double miR-34a targeting virus (53a-CVB) by inserting miR-34a targets in both the 5'UTR and 3'UTR of the virus. 53a-CVB was minimally toxic to cells in normal tissue, but maintained nearly its full oncolytic activity in mice xenografted with human lung cancer. 53a-CVB is the first miR34-regulated OV, and represents a promising platform for the development of safe and effective anti-cancer therapies.

Abbreviation list

OV,	oncolytic virus
TLR,	toll-like receptor
IFN,	interferon
JAK/STAT,	janus kinase/signal transducer and activation of transcription
PKR,	protein kinase R
APC,	antigen-presenting cell
DAMP,	damage-associated molecular pattern
HMGB,	high mobility group box
PAMP,	pathogen-associated molecular pattern
GM-CSF,	granulocyte-macrophage colony-stimulating factor
VV,	vaccinia virus
HSV,	herpes simplex virus
ORF,	open reading frame
UTR,	untranslated region
IRES,	internal ribosomal entry site
ICAM-1,	intracellular adhesion molecule-1
DAF,	decay-accelerating factor
CAR,	coxsackievirus and adenovirus receptor
miRNA,	microRNA
RISC,	RNA-induced silencing complex
miRT,	miRNA target sequence
miR-34aT,	target sequence of miR-34a
miR-34cT,	target sequence of miR-34c
$TCID_{50}$,	median tissue culture infectious dose
AST,	aspartate aminotransferase
ALT,	alanine aminotransferase
BUN,	blood urea nitrogen
LDH,	lactate dehydrogenase
i.t.,	intratumorally
s.c.,	subcutaneously
i.v.,	intravenously

Introduction

Lung cancer became the major cause of cancer deaths among Japanese, making up approximately 25% of all cancer deaths in men and 14% in women (*2*). Five-year survival of lung cancer patients is 39.1% for all stages, despite the use of intensive combined therapies and recent advances in molecular targeting therapies. To improve this poor prognosis, new therapeutic modalities are urgently required.

Oncolytic viruses

In the past decade, oncolytic viruses (OVs) were developed as a new class of therapeutic agents for cancer treatment. These agents exhibit their oncolytic function by their ability to infect, preferentially replicate and kill cancer cells. Although OVs could enter both normal and cancer cell, in normal cells, a variety of signaling pathways work to recognize and eliminate viral infection. Following viral infection, the antiviral machinery can be triggered by Toll-like receptors (TLRs), which recognize invading pathogens or endogenous damage signals and initiate the innate and adaptive immune response (*3*). Once a virus is detected, activation of interferon (IFN) induced Janus kinase/signal transducer and activation of transcription (JAK/STAT) pathway, resulting in limited viral spread and induced apoptosis or necrosis of infected cells (*4*). The local IFN

production can also active protein kinase R (PKR) activity that plays a key role in the innate immune response to viral infection to terminate cell protein synthesis and promote rapid cell death (*5*). In contract, cancer cells show abnormal or dysfunctional innate signaling pathway, such as inhibition of IFN pathway and downregulation of PKR, to evade immune surveillance, and to proceed tumor growth (*6*). This tumor-specific mechanism limits detection of virus by TLR, allowing virus to successfully replicate in tumor cells and fulfill their oncolytic function, resulting in selective lysing of cancer cells. Some OVs also could take advantage of dysregulate apoptotic pathways in cancer cells to shunt cells toward other forms of death. Another character of OVs is biological amplification, which is the key difference from the other traditional drugs. When OVs successfully infect and replicate into the cancer cells, they make copies of itself until cell lysis, followed by release of new infectious viruses from dying cells to infect nearby tumor cells. In additional, the regulation of blood vessel formation located in tumor microenvironment (TME) appears to be an immunosuppressive phenotype by inhibiting the dendritic cells, promoting the proliferation of regulatory T cells (*7*). Many studies showed that OVs can also target and destroy tumor vasculature but leave normal vasculature unbroken to improve their therapeutic efficacy (*8-10*). Finally, the stimulation of patient-specific innate and adaptive immune response with OVs

treatment can enhance antitumor activity. Virus-mediated dead tumor cells release tumor-associated antigens that allow the tumor to be recognized by antigen-presenting cells (APCs). They also release damage-associated molecular patterns (DAMPs, including high mobility group box 1 (HMGB1) protein, heat shock protein, calreticulin and ATP), pathogen-associated molecular patterns (PAMPs), and cytokines (such as IL-12, type I IFN, and tumor necrosis factor-α), resulting in APCs activation. Subsequently, these APCs can trigger the antitumor immune response, recruiting activated macrophages, natural killer cells, $CD4^+$, and $CD8^+$ T cells to TME, resulting in a long-last immunological memory against cancer (*11-13*).

Very recently, talimogene laherparepvec (T-Vec), an oncolytic herpes simplex virus type 1 engineered to contain granulocyte-macrophage colony-stimulating factor (GM-CSF) cDNA, was approved by the Food and Drug Administration of the United States as the first OV immunotherapy for advanced melanoma (*14*). The success of this therapy encourages scientists to make further research on this new field for cancer patients. Various kinds of viruses with natural oncolytic capacity, as well as genetically manipulated virus genome to induce tumor-lysis have been developed and are currently undergoing pre-clinical and clinical studies for many types of cancers (*15*). Among 114 clinical trials currently listed in *clinicaltrials.gov* as of this writing (28-Jan-2019),

3 most widely studied oncolytic viruses are adenoviruses, vaccinia viruses (VVs), and HSV-1 viruses. I) Oncolytic adenovirus has been genetically modified in many strategies of mutations of the E1 gene to enhance its tumor-selective viral oncolysis (*16, 17*), or incorporation with various transgenes (GM-CSF, hTERT, or HSV-thymidine kinase, etc.) to induce apoptosis, both of these serve to stimulate recruitment of immune cell to tumor. II) The development of VV could be traced back to the last 1980s, one of the greatest inventions in medical history: eradication of smallpox (*18*). Since then, VV has been developed as a vector against various infectious diseases as well as in oncolytic virotherapies with genetically modification. The characteristics and life cycle of VV were well written in Smith, GL's review (*19*). III) HSV-1 was genetically engineered with deletion in ICP34.5, which neutralizes the activity of RNA-dependent protein kinase PKR, to attenuate viral pathogenicity and increase tumor-selective replication (*20*), and in ICP47, which is an inhibitor of transporter involved in antigen presentation (*21*). It was also inserted with GM-CSF, an immunestimulatory cytokines that can promote APC recruitment and subsequent induction of tumor-specific T-cell responses (*22*).

However, tumor cells often become resistant to OVs due to dowenregulation of their receptors, leading to insufficient proliferation and transmission of viruses. Therefore, novel OVs targeting

different tumor-expressing receptors with strong proliferative ability would be useful in the clinical setting.

Coxsackievirus B3

To obtain a novel potent OV, our lab previously screened 28 enterovirus strains against 12 different human cancer cell lines for oncolytic activity, and found that coxsackievirus B3 (CVB3) was a highly potent OV capable of targeting a wide range of human tumors, including non-small cell lung cancer (NSCLC) (*1*). Coxsackievirus is a member of genus *Enterovirus* within the *Picornaviridae* family, and is further divided into two groups: coxsackie A with 23 serotypes (CVA1-22, 24), and coxsackie B with 6 serotypes (CVB1-6). It is a non-enveloped virus that is icosahedral in structure, and the capsid encloses a single strand of positive-sense RNA genome (ssRNA), approximately 7.4 kb in length. The ssRNA comprises an open reading frame (ORF) that contains structural proteins (VP1-4) in the P1 region and the non-structural proteins (2A-2C and 3A-3D) in the P2 and P3 regions. The 5' untranslated region (UTR) contains an internal ribosomal entry site (IRES) inside of eukaryotic 7-methylguanosine triphosphate cap, and the 3'UTR of viral genome is 3'-poly(A) tail (*23*, *24*).

Coxsackievirus infection begins by binding of the virus to host-cell receptors: CVA is dependent on binding to both intracellular adhesion molecule-1 (ICAM-1) and decay-accelerating factor (DAF, also known as CD55); while CVB is dependent on binding to both coxsackievirus and adenovirus receptor (CAR) as the main receptor and DAF as secondary functional receptor (*1, 25*). After entering into the cytoplasm, the virus rapidly shut-off host cellular RNA and protein synthesis by virus-encoded proteas 2A via cleaving eIF4G and PABP, which play a central role in cap-dependent translation. In contract, this cleavage does not affect coxsackievirus RNA, because the viral genome is uncapped and contains an IRES in 5'UTR. Then the viral genome is translated into a large single viral protein, followed by cleaving into individual structural proteins and non-structural proteins. Next, non-structural proteins mediate the replication of RNA genome, the newly synthesized viral RNA genome and structural proteins are combined to form new infectious viral particles and released after cell lysis (*26*). Following viral replication, CVB3 could induce caspase-mediated apoptosis and PI3K and MAP/ERK survival signaling pathway to process robust antitumor oncolytic activity (*1*).

Problems

Despite these promising results, safety issues persist: due to its broad tropism, CVB3 mainly infects multiple human organs: heart, pancreas, central nervous system, and cause myocarditis, pancreatitis, and aseptic meningitis (*27-29*). Accordingly, elimination of these virulent features of CVB3 is essential for developing CVB3-based OVs in the clinical setting.

Solution: microRNA-regulated system

Therefore, the aim of this study is to inhibit the virus replication in normal organs and produce a more safety oncolytic virus for clinical trial. For this purpose, these is a solution could be considered: microRNAs (miRNAs)-regulated system. miRNAs are 21-25 nt long endogenous small RNAs. They mainly cause degradation or translational inhibition of mRNAs by guiding the RNA-induced silencing complex (RISC) to mRNA targets, which contain sequences that are complementary to miRNAs, leading to decrease or block protein production (*30, 31*). In addition, the expression profiles of many miRNAs can be clearly distinguished between normal and cancerous cells (*32*). Several reports have shown that the off-target toxicity of OVs can be reduced by inserting miRNA target sequences into the viral genomes (*33-36*). Thus, tissues-specific miRNA (expression-high in normal tissue and expression-low in cancer tissue) could be considered to be useful to control the undesirable tropism of CVB3, gaining safer and more effective antitumor treatment.

As TP53 was well-known to tumor suppressor mainly affected by oncogenic stress and DNA damage, Lin He and his colleagues compared the expression of a total 145 miRNAs in wild-type and p53-deficient cells and identified that miR-34 family was transcriptionally activated by TP53 (*37*). We therefore focused on miR-34 family which comprises three members: miR-34a, miR-34b, and miR-34c. miR-34a located on chromosome 1p36.22, whereas miR-34b and miR-34c share a common precursor transcript located on chromosome 11q23.1. And then many reports showed that miR-34a was expressed in most normal tissues, and miR-34b and miR-34c were expressed predominantly in normal lung and brain (*38-40*). But all members of miR-34 family was frequently repressed in various tumor types compared with normal tissue due to the role of miR-34 family in induction of apoptosis and differentiation, and inhibition of cell cycle.

Hypothesis

Therefore, I hypothesized that insertion of target sequences for miR-34a (miR-34aT) and miR-34c (miR-34cT) in the CVB3 genome would reduce pathogenesis of CVB3 (Table 1). I demonstrated that CVB3 harboring a miR-34 target sequences could be useful for cancer treatment. This is the first report to demonstrate the effectiveness of miR-34–controlled gene regulation in an OV.

Table 1. Summary of the correlation between the receptor, tropism, pathogenicity of CVB3 and expression of miR-34.

Organs	Receptors (CAR)	Tropism	Pathogenicity	Expression of miR-34a	Expression of miR-34c
brain	++	+	aseptic meningitis / meningoencephalitis	++	+++
heart	+++	+	myocarditis	+++	+
lung	+	-	-	++	+++
liver	++	+	fulminant hepatitis	+	-
pancreas	+++	+	pancreatitis	++	-
spleen	-	+	-	+	-
kidney	+	-	-	++	+
intestines	+++	-	-	+	-

CAR: coxsackievirus and adenovirus receptor. The biodistribution of CAR in various organs depends on previous studies (*41*, *42*). The data of tropism and pathogenicity of CVB3 are from previous studies (*27*, *43*). The data of miR-34 expression is from previous studies (*38-40*) and this study (Figure 2).

Materials and methods

Mice

Four- to five-week-old female BALB/c nude mice and C57BL/6J mice were purchased from Oriental Yeast (Tokyo, Japan). All animal experiments were carried out under the Guidelines for Animal Experiments of The University of Tokyo and Law 105 Notification 6 of the Japanese Government.

Cell lines

Non–small cell lung carcinoma (NSCLC, NCI-H1299), pancreatic cancer (AsPC-1), cervical adenocarcinoma (Hela), and human normal lung bronchial epithelium (BEAS-2B) cell lines were purchased from the American Type Culture Collection (Manassas,VA, USA). Lung carcinoma (A549) cell line was purchased from Riken Cell Bank (Wako, Japan).

Construction pf miR-34a/cT-containing CVB (miRT-CVB) plasmids

A plasmid coding full-length CVB3 (Nancy strain) infectious clone cDNA, pBluescript II KS-CVB3 was used as the starting material for genetic manipulations. To insert miR-34a/cT in CVB

cDNA, pBluescript II KS-CVB3 was first linearized by PCR (94℃ for 2 min; 30 cycles of 98°C for 10 sec, 60°C for 30 sec, and 68°C for 6 min; and finally 72°C for 7 min), then treated with *Dpn*I (TOYOBO, Osaka, Japan) for one hour at 37°C to digest residual template plasmid. To prepare insert fragments of miR-34a/cT or miR-39T (control), synthetic DNA oligomers (Table 2) were usewd as templates of PCR, and the primers for each miR-34a/cT are showed in Table 3. Following the PCRs, the vector was purified by gel extraction (approximately 10 kb), and the linearized vectors and inserts were ligated using the In-Fusion HD Cloning Kit (Takara Bio, Kusatsu, Japan). The closed circular plasmid clones were obtained by transformation with DH5α (TOYOBO). The insertion of miR-34a/cT or miR-39T was confirmed by sequence analysis.

Production of miRT-CVB virus stocks

The miRT-CVB plasmids were linearized with *Sal* I-HF (NEB, Ipswich, MA, USA), and the reaction was terminated by adding 1/10 volume of ammonium acetate solution (5M) and two volumes of ethanol. Transcription reaction was performed using the MEGAscript T7 Transcription kit (Thermo Fisher Scientific, Waltham, MA, USA) and purified by phenol/chloroform extraction followed by ethanol precipitation. H1299 cells were transfected with 50 μg RNA of each virus

Table 2. Sequences of synthetic miR-34a/c target DNA oligomers.

miRT	Inserted sequence (5’ -3’)
miR-34aT x 4	ACAACCAGCTAAGACACTGCCAcgatACAACCAGCTAAGA CACTGCCAaccggtACAACCAGCTAAGACACTGCCAtcacACA ACCAGCTAAGACACTGCCA
miR-34cT x 4	GCAATCAGCTAACTACACTGCCTcgatGCAATCAGCTAACT ACACTGCCTaccggtGCAATCAGCTAACTACACTGCCTtcacGC AATCAGCTAACTACACTGCCT
miR-39T x 4 (Control)	CAAGCTGATTTACACCCGGTGAcgatCAAGCTGATTTACAC CCGGTGAaccggtCAAGCTGATTTACACCCGGTGAtcacCAAG CTGATTTACACCCGGTGA

Uppercase letters represent the miRNA target sequences, and lowercase letters represent spacer elements.

Table 3. Primer sequences for miR-34a/cT PCR

Primer	Sequence (5'- 3')
5a-CVB-forward	AACCAGCTAAGACACTGCCAATGGGAGCTCAAGTATCAAC
5a-CVB-reverse	GCAGTGTCTTAGCTGGTTGTTTTGCTGTATTCAACTTAACAATG
5c-CVB-forward	ATCAGCTAACTACACTGCCTATGGGAGCTCAAGTATCAAC
5c-CVB-reverse	CAGTGTAGTTAGCTGATTGCTTTGCTGTATTCAACTTAACAATG
3a-CVB-forward	AACCAGCTAAGACACTGCCAGAGACAATTTGAAATAATTTAGATTGG
3a-CVB-reverse	GCAGTGTCTTAGCTGGTTGTTAATCTAAAAGGAGTCCAACC
3c-CVB-forward	ATCAGCTAACTACACTGCCTGAGACAATTTGAAATAATTTAGATTGG
3c-CVB-reverse	CAGTGTAGTTAGCTGATTGCTAATCTAAAAGGAGTCCAACC

using Lipofectamine 3000 (Thermo Fisher Scientific). Twenty-four to thirty hours after transfection, the culture medium was collected and used to inoculate H1299 cells. After 6–10 hrs, the cells were collected with a cell scraper followed by three freeze–thaw cycles, and then the cell lysate was centrifuged to separate cell debris. The supernatants were collected as virus stocks and the aliquots were stored at -80°C.

Virus titration and single-step growth curve analysis

H1299 cells (5×10^3 cells/well) were seeded into 96-well plates and incubated at 37°C for 8 hrs. Ten-fold serial dilutions of each virus stock were prepared, and 50 μl of each dilution was added to each of eight replicate wells. After 5 days of culture, cell lysis in each well was evaluated by crystal violet, as described above, and the titer was calculated by $TCID_{50}$ using the following formula: log10 (TCID50/ml) = L+d (S-0.5) +log10 (1/v). L = most concentrated virus dilution; d = log10 of dilution factor; S = sum of individual proportions; v = volume of add virus/well = 0.05ml. To determine the replication of CVBs in H1299 or BEAS-2B cells, with or without miR-34a or miR-34c transfection, the cells were subjected to single-step growth curve analysis. Briefly, the cells were inoculated with viruses at an MOI of 3 for 1 hr and therefore medium was replaced to

fresh medium. At 6, 12, 24, and 48 hrs after the infection, cells and supernatants were harvested and stored at -80℃ until use. Then, all samples were subjected to freeze-thaw treatment for three times and cell debris was removed by centrifugation. The supernatant was used for titration with H1299 cells, as described above.

RT-qPCR of miRNA

To determine expression levels of miR-34a/c in culture cells and mouse organs, total microRNA was extracted from cells or mouse organs using the mirVana miRNA Isolation Kit (Thermo Fisher Scientific). For microRNA quantitative PCR, cDNA was synthesized from total microRNA using TaqMan MicroRNA Reverse Transcription Kit (Thermo Fisher Scientific). Subsequently, real-time PCR was carried out using TaqMan Universal PCR Master Mix (Thermo Fisher Scientific) to detect levels of mature miR-34a/c. U6 snRNA was used as the endogenous control. Fold changes were calculated by relative quantification ($2^{-(\Delta\Delta Ct)}$ method).

Crystal violet staining

Cells were infected with viruses at appropriate multiplicity of infection (MOI) for 1 hr, and then the viral supernatant was replaced with fresh media. After 72 hrs, the cells were incubated with 300 µl of 0.5% glutaraldehyde per well as a fixative for 10 minutes, and then stained with 300 µl of 0.1% crystal violet per well for 10 – 15 min, followed by washing twice with PBS.

miRNA mimics transfection experiment

miRNA oligonucleotide mimics were purchased from Bioneer Corporation (Bioneer, Daejeon, Korea). miRNA mimics were transfected into H1299 cells using Lipofectamine RNAiMAX (Thermo Fisher Scientific) at a concentration of 10 µM. Twenty-four hours later, the copy numbers of miR-34a/c were determined by RT-qPCR, as described above. The transfected cells were inoculated with viruses at an MOI of 10^{-4} to 1, and the cells were subjected to crystal violet staining after 72 hrs, as described above.

MTS assay for cell viability

In vitro cell viability was measured using cells (1×10^6) infected with miRT-CVBs by MTS assay using CellTiter 96 AQ_{ueous} One Solution Cell Proliferation Assay (Promega, Madison, WI, USA)

following manufacturer's protocol. To determine the effect of cellular signaling pathway inhibitors on the cytotoxicity of miRT-CVBs, cells were pretreated with 2% FBS media containing 10 μM of MEK1/MEK2 inhibitor PD0325901 (Wako Pure Chemical, Osaka, Japan) or 10 μM of PI3K inhibitor LY294002 (Santa Cruz Biotechnology, Dallas, TX, USA) for 1 hr, and then inoculated with miRT-CVBs at an MOI of 10. Sixteen hours after infection, an MTS assay was performed, as described above.

Quantification of CVB3 copy numbers in mouse organs

To quantify miRT-CVB genome, mouse organ samples were collected for the RNA extraction by using RNeasy Plus Mini Kit (QIAGEN, Germany). To obtain cDNA, reverse transcription for twenty nanograms of the total RNA was performed with ReverTra Ace qPCR Master Mix (TOYOBO). Subsequently, 2/100 volume of cDNA was subjected to real-time PCR by using PrimeTime Gene Expression Master Mix (Integrated DNA Technologies, USA) and CVB genome specific primers (forward: 5'-GTGCAAGGCCCTGCCTTT-3'; reverse: 5'-AACGGCCCACCTGTCATAGA-3') according to the manufacturer's protocol. pBluescript II KS-CVB3 was used to create the standard curve for the calculation of the viral copy numbers.

Since one copy of the plasmid is 6.8×10^6 (= 10,318 bp × 660) Da, 1 ng of the plasmid contains 8.85×10^7 (= $1 \times 10^{-9} \times 6.023 \times 10^{23} / 6.8 \times 10^6$) copies of virus genome.

In vivo therapeutic studies

To establish xenograft mouse models, 5×10^6 H1299 cells were injected subcutaneously (s.c.) into the right flank of BALB/c nude mice. To establish immunocompetent mouse tumor models, 1×10^5 TC-1 cells were injected s.c. into the C57BL/6J mice. After 2 days, when tumor size reached 0.5 cm in diameter, 5×10^6 $TCID_{50}$ WT-CVB, miRT-CVBs or vehicle (Opti-MEM, Thermo Fisher Scientific) was injected into the tumors. For multiple injection studies, miRT-CVBs or vehicle were injected intratumorally on days 2, 4, 6, 8, and 10 for the total of five times. Tumor size and body weight were measured every other day for 60 days after tumor transplantation, and tumor volume was calculated as length × width × width/2. Mice were euthanized when the diameter of tumors exceeded 1.0 cm or signs of skin ulceration were evident. To address safety issues, the mice were euthanized 2 days after virus injection, and whole blood, heart, liver, and pancreas were collected for biochemical and histopathological analysis.

Biochemical analyses

BUN, AST, ALT, T-Bil, amylase, and LDH levels in mouse serums were measured using a blood biochemistry analyzer (Arkray SPOTCHEM EZ-SP-4430, Kyoto, Japan).

Histopathological examination

Mouse organs were fixed in formalin for 24 hrs, washed five times with PBS, and then dehydrated in 75% alcohol. The organs were embedded in paraffin and processed for sectioning and H–E staining by the Pathology Core Laboratory of the Institute of Medical Science, The University of Tokyo (IMSUT). Sections were observed and diagnosed by a pathologist at IMSUT Hospital using a BZ-9000 fluorescence microscope (KEYENCE, Osaka, Japan).

Statistical analysis

All statistical analyses and graphical representations were performed using GraphPad Prism software, version 5.0a (GraphPad Prism, USA). Survival curves were plotted according to the Kaplan–Meier method, and statistical differences were evaluated by log-rank test. The results of MTS and biochemical analyses were compared by one-way ANOVA (Tukey's Multiple

Comparison Test, and Dunnett's Multiple Comparison Test). All differences were considered statistically significant at a $p < 0.05$.

Results

Expression of miR-34a and miR-34c in cancer cells and normal tissues. To determine the expression levels of miR-34a and miR-34c in cancer and normal cells, we first examined a non–small cell lung cancer H1299 and normal bronchial epithelium BEAS-2B cells for expression the both miR-34a and miR-34c, using reverse transcription quantitative PCR (RT-qPCR) (Figure 1). H1299 cells expressed much lower levels of miR-34a than BEAS-2B cells. We also examined miR-34a expression in normal organs of mice, and found that it was expressed at higher levels in all organs, particularly in brain, pancreas, heart, and lung, than in H1299 cells. Brain and lung also expressed miR-34c abundantly (Figure 2).

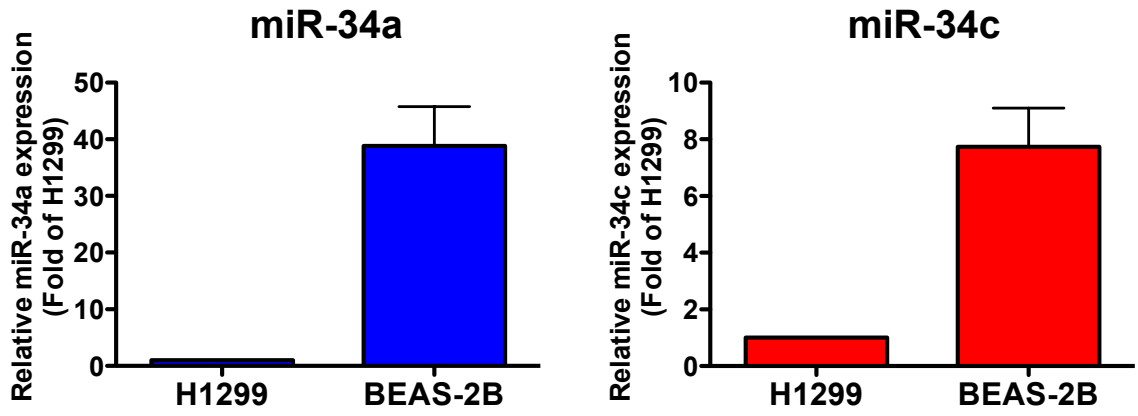

Figure 1. Expression levels of miR-34a and miR-34c in H1299 and BEAS-2B cells.

H1299, human NSCLC cell line; BEAS-2B, human normal bronchus epithelium cell line. Values were measured by RT-qPCR and normalized against U6 snRNA. Data represent means ± standard deviation (SD) of triplicate assays.

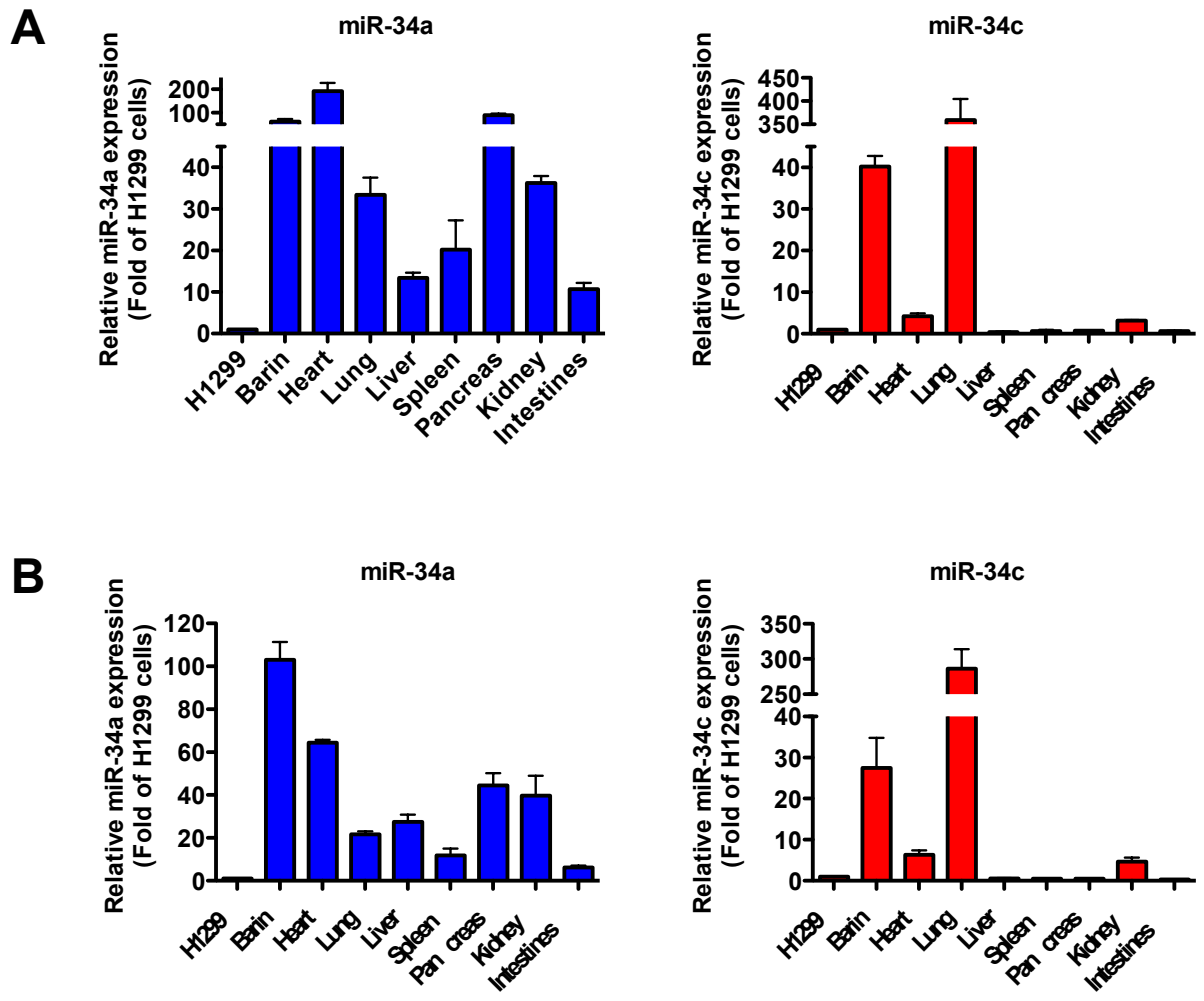

Figure 2. Expression levels of miR-34a and miR-34c in mouse organs.

Values were measured by RT-qPCR and normalized against U6 snRNA. Data represent means ± standard deviation (SD) of triplicate assays.（A） represents C57BL/6 mouse; (B) represents BALB/c nude mouse.

Insertion of miRNA target sequences in 5'UTR or 3'UTR of CVB3 genome. These results suggested that insertion of miR-34aT or miR-34cT into the CVB3 genome would suppress viral translation and proliferation in normal cells expressing these miRNAs. Based on previous reports about insertion-tolerant sites of picornaviruses (*44, 45*), we predicted that miRNA target sequences (miRTs) could be inserted in the 5' region immediately upstream of the start codon, as well as in the 3' region just downstream of the stop codon. In addition, insertion of four copies of miRT in viral vector genomes can be efficiently controlled by complementary miRNAs (*46*). Therefore, we engineered miRNA-regulated CVB3s (miRT-CVBs) by inserting four tandem miR-34aTs or miR-34cTs into the 5'UTR (ntd 743) (5-CVBs: 5a-CVB and 5c-CVB) or 3'UTR (ntd 7,305) (3-CVBs: 3a-CVB and 3c-CVB) of the CVB3 genome (Figure 3). We also constructed control CVB3s (Ctrl-CVB) by inserting a miRNA target gene corresponding to *C. elegans* miR-39, which does not exist in mammalian cells, in the 3'UTR as 3-CVB.

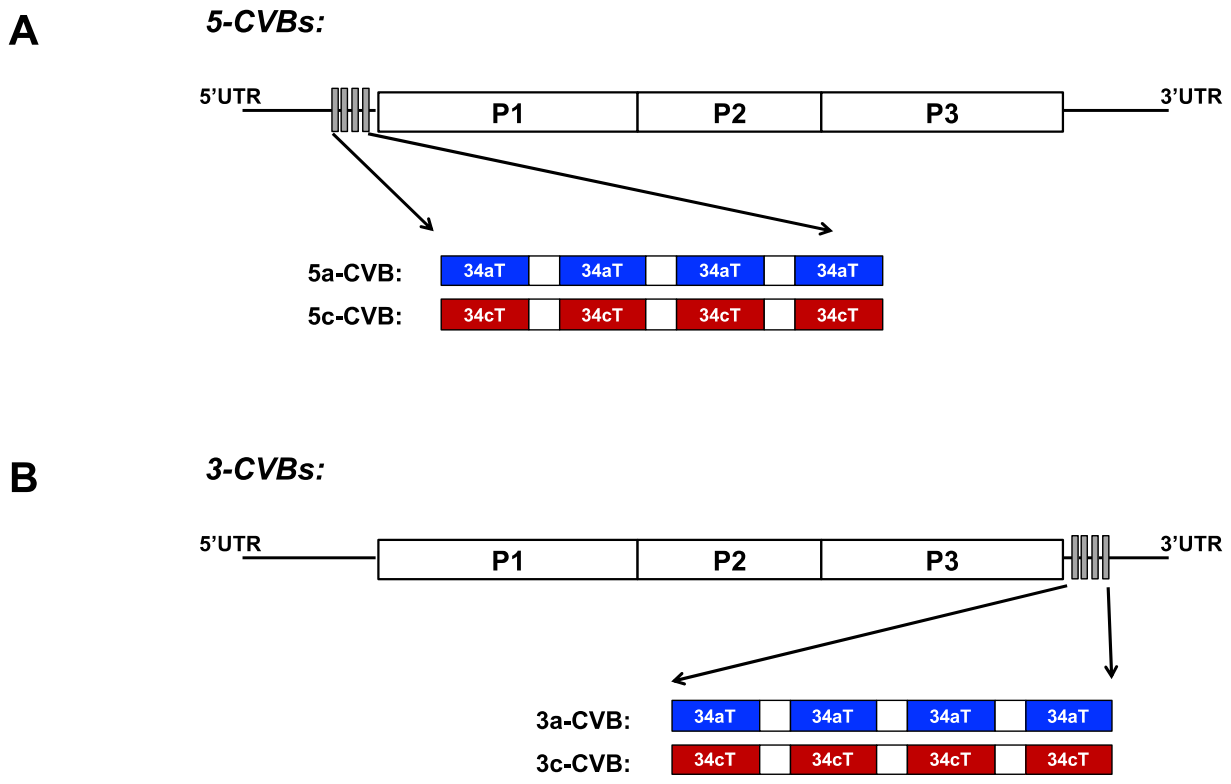

Figure 3. Schematic diagram of miRT-CVBs.

A. Four tandem insertion sites of miR-34aTs (34aT) or miR-34cTs (34cT) constructed in 5'UTR of CVB3 genome.

B. Four tandem 34aT or 34cT constructed in 3'UTR of CVB3 genome.

Improved tumor specificity of CVB3 by inserting miRTs in UTRs. To examine the effect of miRT insertion in the CVB3 genome on cytotoxicity, we transfected synthetic miR-34a or miR-34c mimics to H1299 cells. After confirming successful transfection of both miRNA mimics at almost the same level, the cells were inoculated with miRT-CVBs (Figure 4). Seventy-two hours later, the cells were stained with crystal violet. In untransfected H1299 cells, all miRT-CVBs induced massive cell lysis, as did wild-type (WT-CVB) in a dose-dependent manner even at MOI of 10^{-4} (Figure 5A, left panel), which is the limitation of WT-CVB oncolytic activity (Figure 5B). By contrast, H1299 cells transfected with miR-34a or miR-34c exhibited much less cell lysis when infected with miRT-CVBs harboring complimentary miRTs. 3-CVBs exhibited less cytotoxicity than 5-CVBs, and miRT-CVB with miR-34aT exhibited less cytotoxicity than miRT-CVB with miR-34cT (Figure 5A, middle and right panels). These results indicated that insertion of miRTs made CVB3 less toxic only in cells expressing miR-34a or miR-34c.

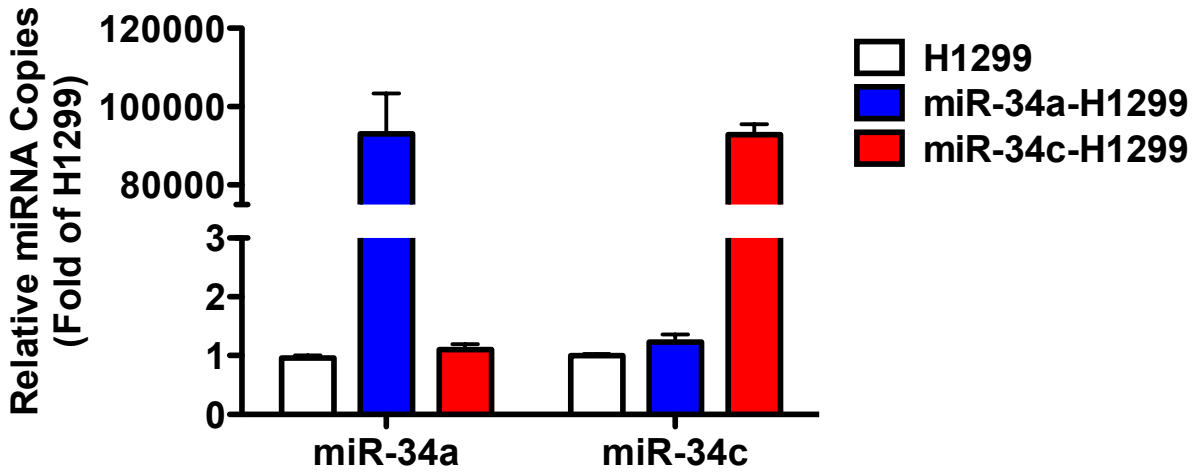

Figure 4. Relative copy numbers of miR-34 mimics in transfected H1299 cells.

H1299 cells were transfected with 10 μM miR-34a (miR-34a-H1299) or miR-34c (miR-34c-H1299) mimics by using Lipofectamine RNAiMAX. 24 hrs later, relative copy numbers of of miR-34a and miR-34c were measured by RT-qPCR and normalized against U6 snRNA. Data represent means ± SD of triplicate assays.

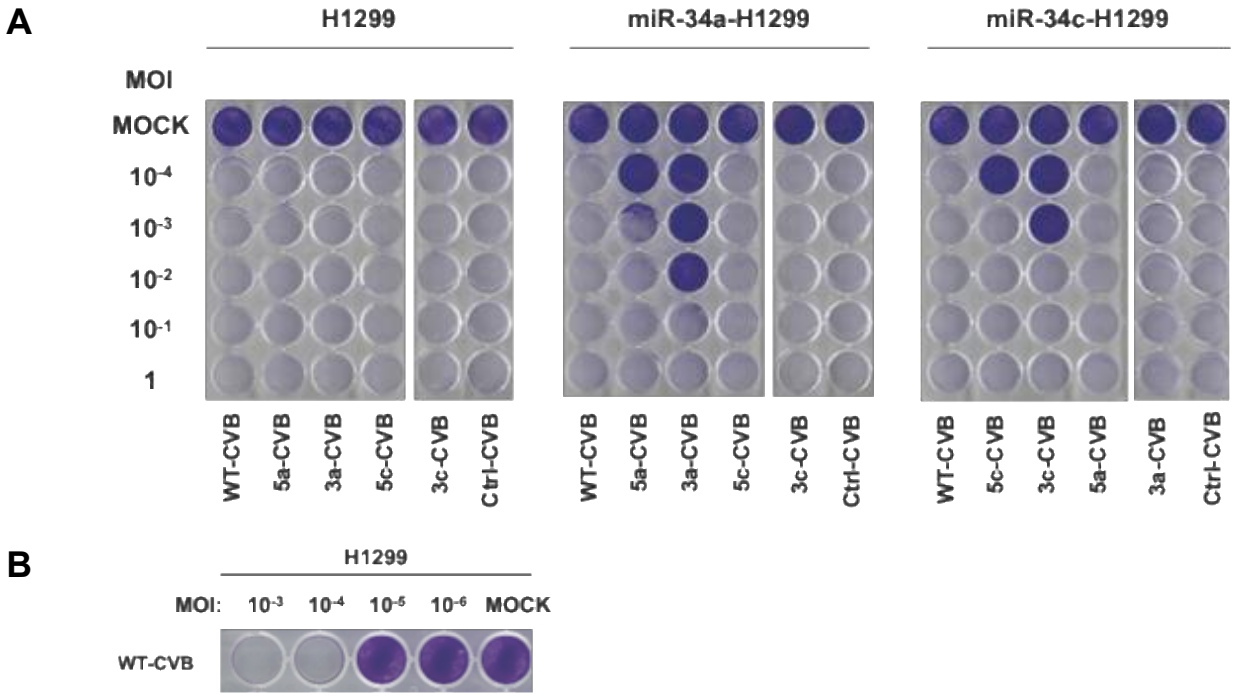

Figure 5. Cytotoxicty of miRT-CVBs in miRNA mimic-transfected cells.

(A) Representative images of H1299 cells transfected with miR-34a/c mimics, followed by inoculation with indicated viruses at an MOI of 10^{-4} to 1. (B) Representative images of H1299 cells inoculated with WT-CVB at an MOI of 10^{-6} to 10^{-3}. Cytotoxicity of each virus was determined 72 hrs post-infection by crystal violet staining. All experiments were repeated at least three times.

To further examine the effect of miRT-CVB3s on tumor and normal cells, we inoculated WT-CVB or miRT-CVBs into several tumor cell lines, including H1299, A549, HeLa, and AsPC, as well as BEAS-2B. All tumor cells expressed less miR-34c than BEAS-2B cells, but A549 and HeLa cells expressed higher levels of miR-34a than BEAS-2B cells (Figure 6). As expected, 5c-CVB and 3c-CVB exhibited strong cytotoxicity, comparable to that of WT-CVB in all tumor cells, even at an MOI of 0.001 (Figure 7). Moreover, 5a-CVB and 3a-CVB unexpectedly induced strong cytotoxicity in miR-34a-high A549 and HeLa cells, as well as in miR-34a-low H1299 and AsPC cells (Figure 6). Normal bronchus epithelium BEAS-2B cells were much more resistant to WT-CVB than tumor cells, but at a 100-fold higher titer (MOI of 0.1), only 30% of cells survived (Figure 7). Importantly, in contrast to the results of tumor cells, the majority of miRT-CVBs exhibited reduced cytotoxicity in BEAS-2B cells (Figure 6). 5a-CVB resulted in 60% viability, whereas the cytopathic effect of 5c-CVB was almost the same as that of WT-CVB. In addition, more than 80% of cells survived when inoculated with 3-CVBs. These findings suggest that insertion of miR-34aT or miR-34cT into the 3'UTR of CVB3 genome is an effective strategy for reducing cytotoxicity in normal cells without losing anti-tumor activity.

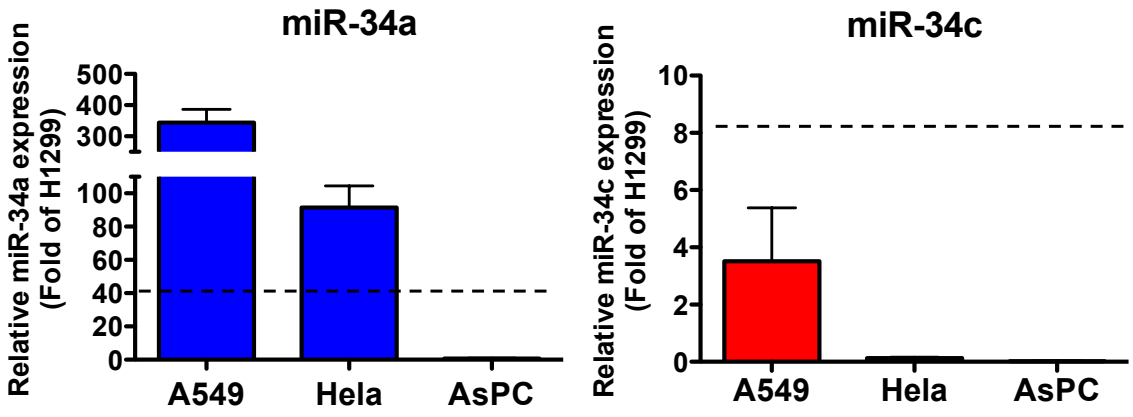

Figure 6. Expression levels of miR-34a and miR-34c in human cancer cell lines.

A549, NSCLC; Hela, cervical cancer cell line; and AsPC, pancreatic cancer cell line. Values were measured by RT-qPCR and normalized against U6 snRNA. Data represent means ± standard deviation (SD) of triplicate assays, and dotted lines indicate average level of BEAS-2B cells.

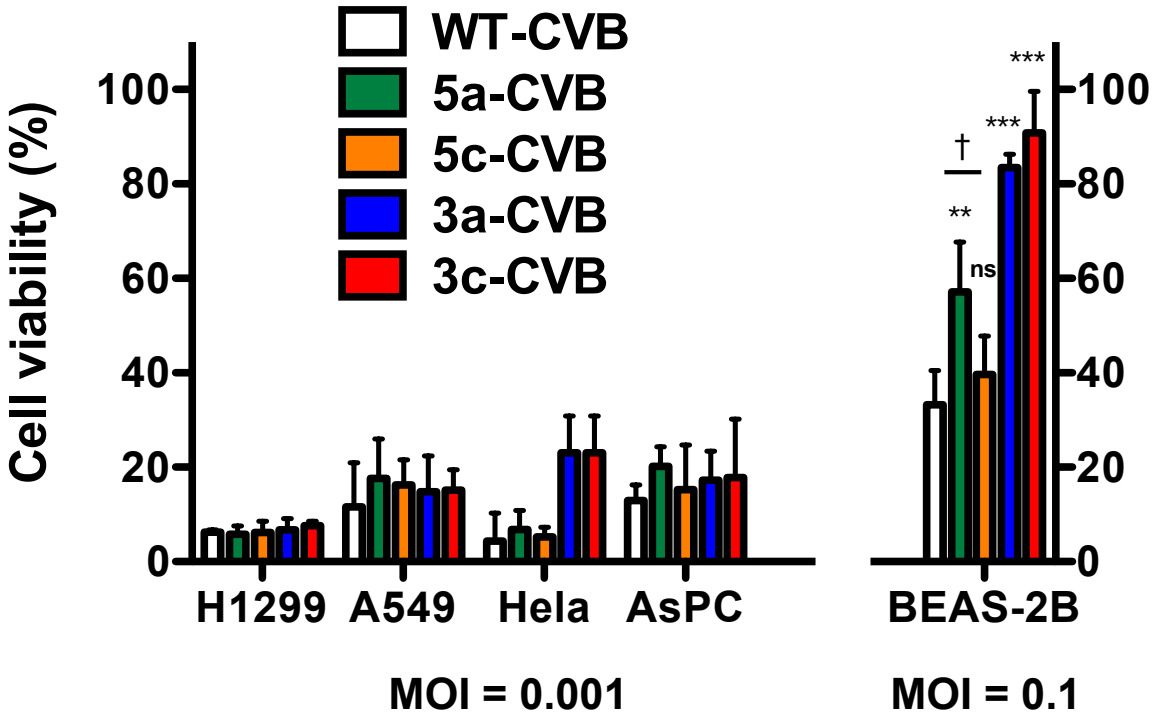

Figure 7. Cell viability of cancer cell lines and BEAS-2B infected with miRT-CVBs.

Cell viability of cancer cell lines and BEAS-2B was determined by MTS assay 72 hrs after inoculation with the indicated viruses at an MOI of 0.001 or 0.1. A549, NSCLC; Hela, cervical cancer cell line; and AsPC, pancreatic cancer cell line. Data represent means ± SD of relative viable cell number vs. un-infected cell number from triplicate assays. **, $p < 0.01$; ***, $p < 0.001$ vs. WT-CVB (Tukey's test). †, $p < 0.05$ 5a-CVB vs. 5c-CVB (Tukey's test).

Anti-tumor activity of miRT-CVB3s in mouse tumor models. To investigate the anti-tumor activity of miRT-CVBs *in vivo*, we injected miRT-CVBs into tumors derived from H1299 cells transplanted into BALB/c nude mice. After subcutaneously transplanted tumors reached 0.5 cm in diameter on day 2, we injected miRT-CVBs or WT-CVBs intratumorally (i.t.) at 1×10^6 $TCID_{50}$ on days 2, 4, 6, 8, and 10. Control mice exhibited continuous tumor growth, whereas all virus-treated groups exhibited complete tumor regression (Figure 8) with no death during the observation period, indicating that miRT-CVBs were preserving anti-tumor activities as effectively as the original WT-CVB (Figure 9). Importantly, although transient weight loss was observed in WT-CVB–treated mice and 5-CVBs after the injections started, no weight loss was observed in 3-CVB–treated mice, suggesting that the toxicity of 3-CVBs was reduced in non-tumor tissues (Figure 10).

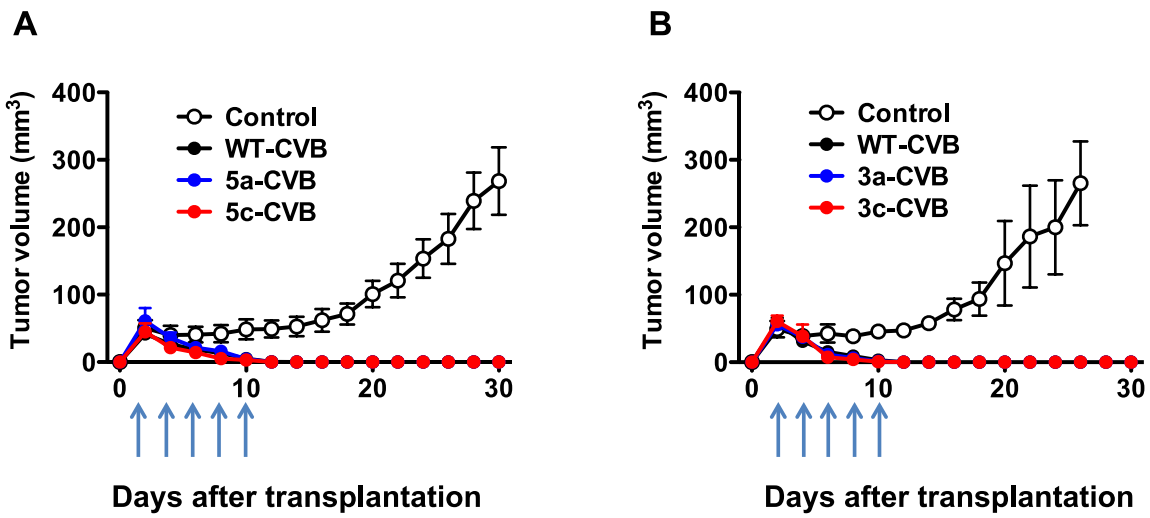

Figure 8. Effect of 5-CVBs and 3-CVBs on growth of H1299 xenograft tumors.

BALB/c nude mice received s.c. transplantation of 5×10^6 H1299 cells. Arrows indicate the timing of five doses (5×10^6 $TCID_{50}$) of i.t. injection of 5-CVBs (A), 3-CVBs (B), WT-CVB, and vehicle control. Tumor volume was measured every 2 days. Data represent means ± SD of each group.

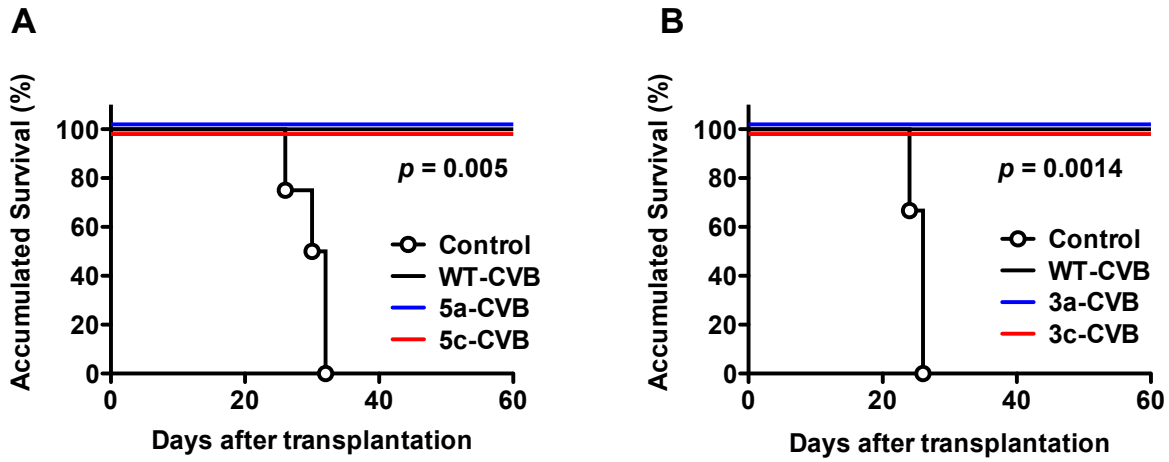

Figure 9. Overall survival of H1299-transplanted mice treated with 5-CVBs (A) or 3-CVBs (B).

Kaplan–Meier survival curves of mice treated with indicated CVBs are shown. *p*, statistical difference between the control group and each virus-treated group calculated by log–rank test.

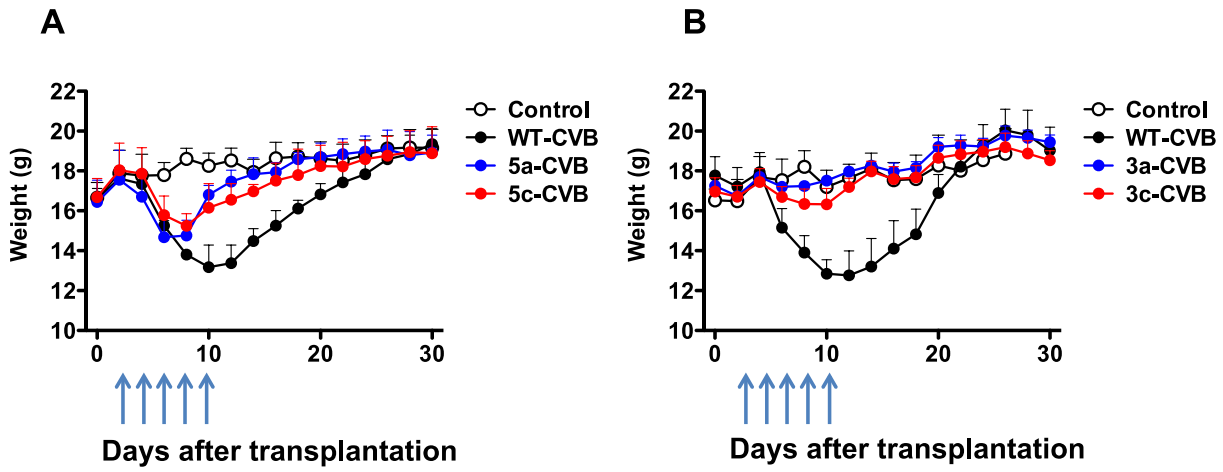

Figure 10. Body weight of H1299-transplanted mice treated with 5-CVBs (A) or 3-CVBs (B). Body weight was measured every 2 days. Data represent means ± SD. Each group consists of four or five mice.

Reduced normal organ injury by miRT-CVBs treatment. To determine whether insertion of miRTs in 5'UTR or 3'UTR could alleviate WT-CVB–associated pathogenicity, we performed blood biochemistry tests and pathological examination of our xenograft mouse models. Nude mice received a single i.t. injection of viruses (1×10^6 $TCID_{50}$) 2 days after inoculation of H1299 cells, and blood samples and mouse organs were collected 2 days after virus injection. In WT-CVB–treated mice, serum AST, ALT, LDH, and amylase levels were significantly increased (Figure 11), and histological signs of pancreatic injury, such as destruction of acinar cells and mononuclear cell infiltration were observed (Figure 12, 13). Although 5-CVBs failed to reduce the WT-CVB–associated pathogenicity (Figure 11A, 12), 3-CVBs significantly showed reduced level of any enzyme except ALT, and induced mild mononuclear cell infiltration resulting in less pancreatic injury (Figure 11B, 13). (Figure 11B, 13). There was no significant difference in serum enzyme levels between 3a-CVB– and 3c-CVB–treated mice. Because elevated LDH reflects to damage of many organs, the reduced LDH elevation in 3-CVB–treated mice could have resulted from restriction of virus replication in a wide range of organs. Moreover, there were no significant changes in serum BUN or total bilirubin (T-bil) levels in all mice treated with any types of CVBs (Figure 14). Although CVB3 has been reported to cause some pathological changes in mouse heart

tissue (*45, 47, 48*), we did not observe any significant pathological findings in the heart, such as myocardial necrosis or inflammation, in mice treated with any type of virus, including WT-CVB (Figure 15,16). In addition, we did not observe any pathological findings in the livers of any mice (Figure 17,18). These results indicated that 3-CVBs are safer than 5-CVBs and WT-CVB, and that in particular 3a-CVB was the best miRT-CVB in terms of anti-tumor effect and safety, although this virus still induced mild ALT elevation.

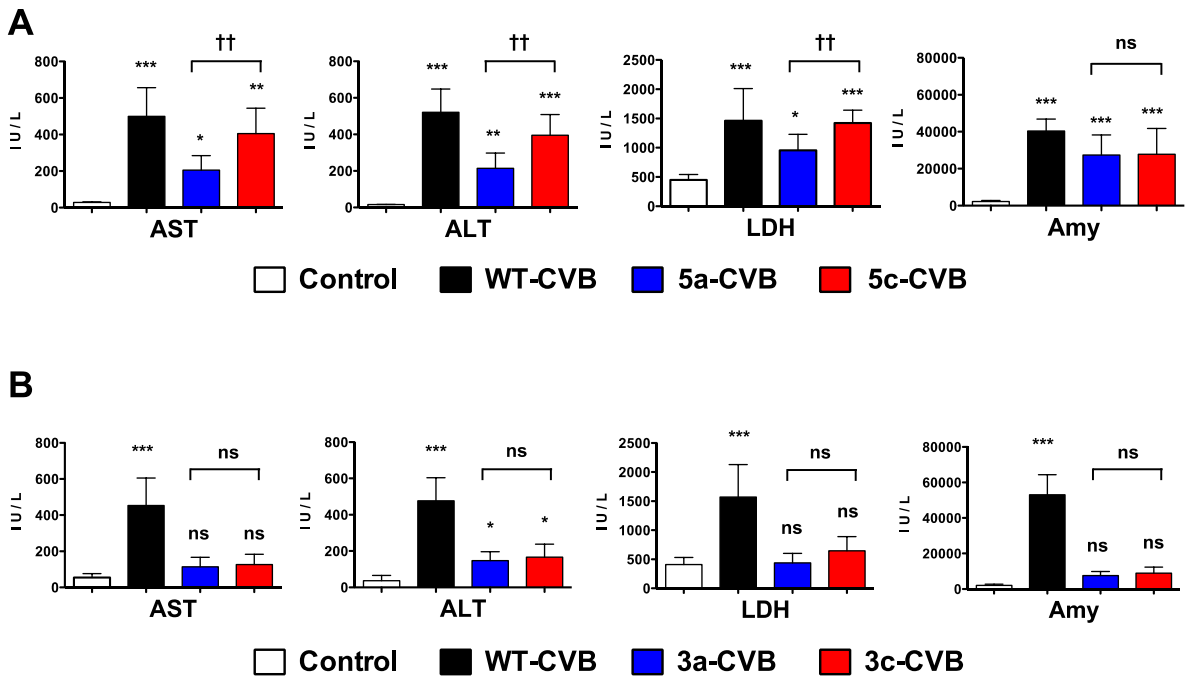

Figure 11. Blood biochemistry tests of mice treatment with 5-CVBs (A) or 3-CVBs (B). H1299 cells (5×10^6) were transplanted s.c. into BALB/c nude mice, and then vehicle control or indicated viruses were inoculated at 5×10^6 $TCID_{50}$ 2 days after transplantation. Blood samples were collected two days after inoculation, and serum ALT, AST, LDH, and amylase levels were measured. Data represent means ± SD of eight or nine mice in each group. *, $p < 0.05$; **, $p < 0.01$; ***, $p < 0.001$ vs. control group (Tukey's test). ††, $p < 0.01$ 5a-CVB vs. 5c-CVB group (Tukey's test).

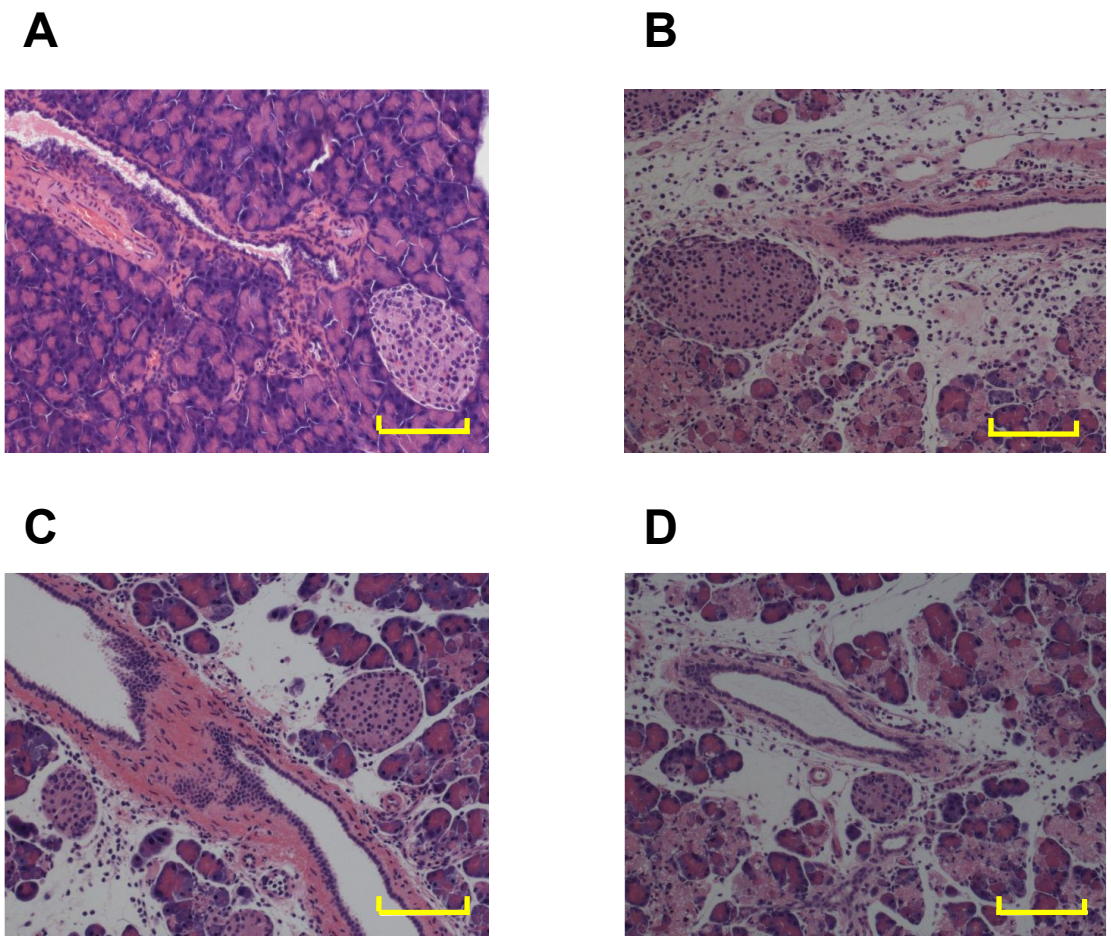

Figure 12. Pathological examination of pancreas from mice treated with 5-CVBs.

Pathological images of pancreas two days after inoculation with vehicle control (A), WT-CVB (B), 5a-CVB (C), and 5c-CVB (D). Magnification: 10× + 2× zoom. Scale bar, 100 μm. All experiments were repeated twice.

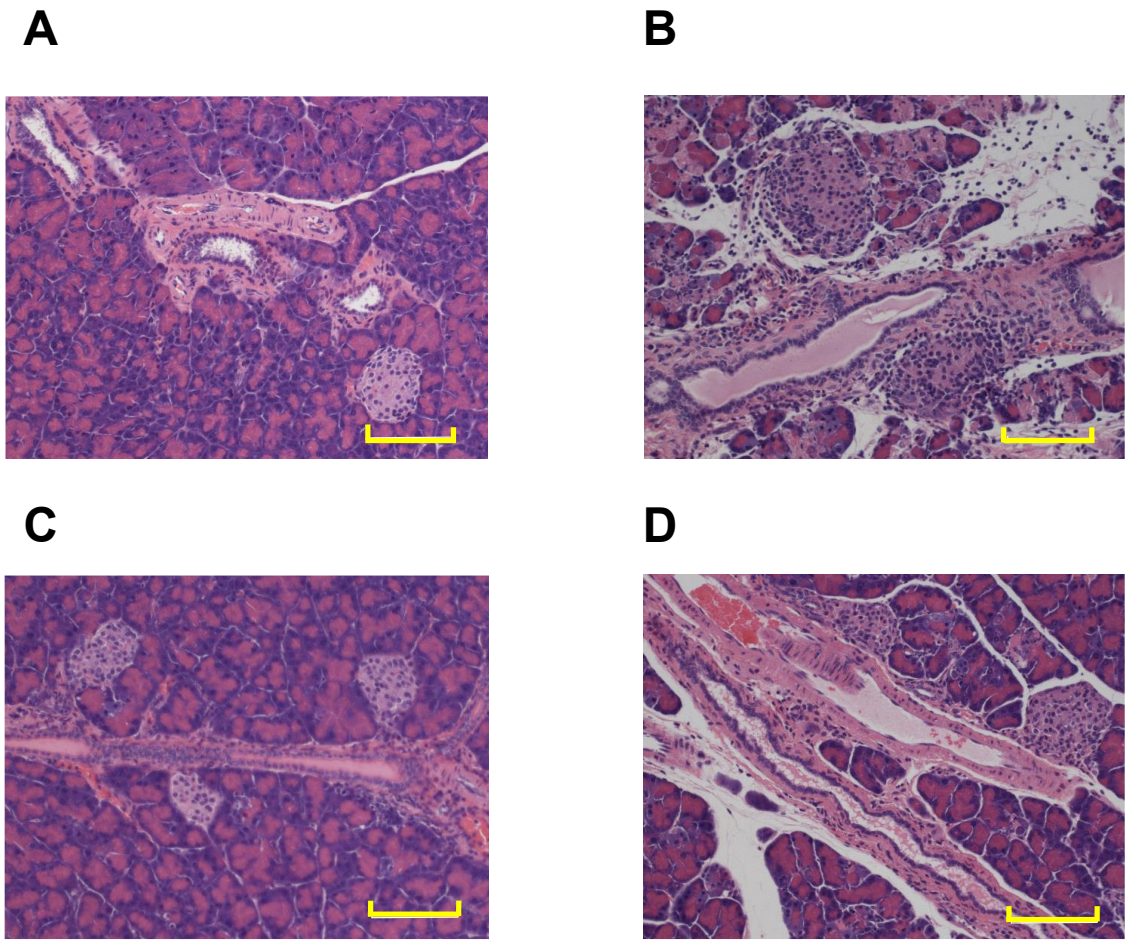

Figure 13. Pathological examination of pancreas from mice treated with 3-CVBs.
Pathological images of pancreas two days after inoculation with vehicle control (A), WT-CVB (B), 3a-CVB (C), and 3c-CVB (D). Magnification: 10× + 2× zoom. Scale bar, 100 µm. All experiments were repeated twice.

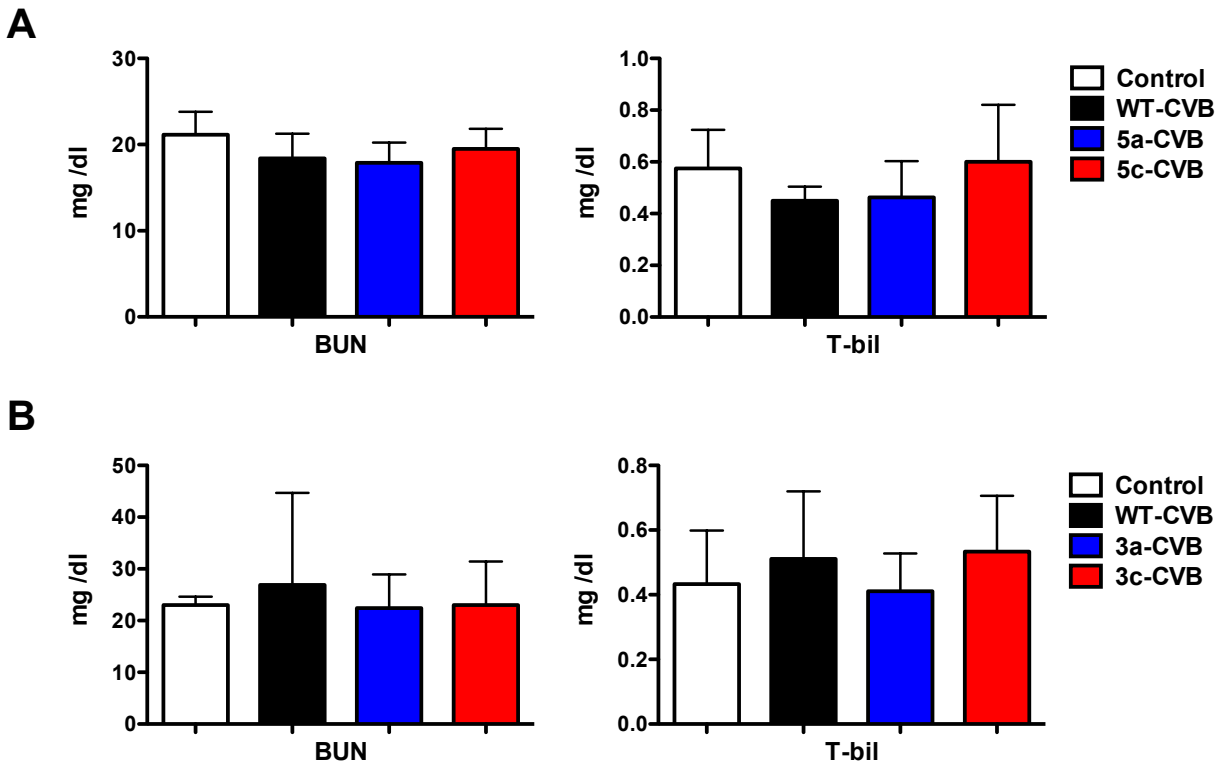

Figure 14. Serum levels of BUN and T-bil in mice treated with 5-CVBs (A) or 3-CVBs (B). Mouse blood samples were collected 2 days after infection, followed by immediate analysis of serum BUN and T-bil. Results are shown for mice treated with indicated CVBs. Data represent means ± SD of eight or nine mice in each group. There are no statistically significant difference between each group by ANOVA.

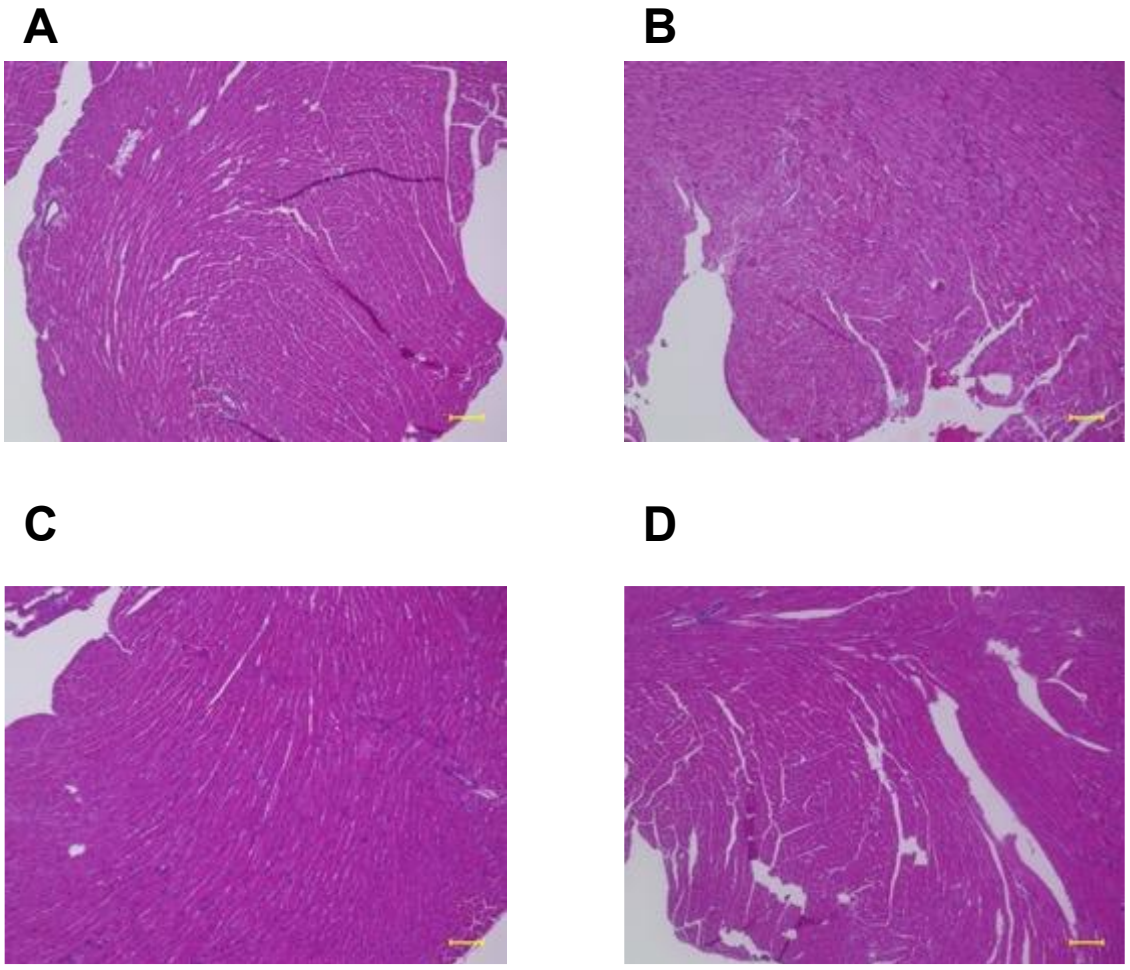

Figure 15. Histological images of hearts from mice treated with 5-CVBs.

H-E staining of hearts isolated from mice treated with vehicle control (A), WT-CVB (B), 5a-CVB (C), and 5c-CVB (D) two days after inoculation. Magnification: 10×. Scale bars, 100 μm.

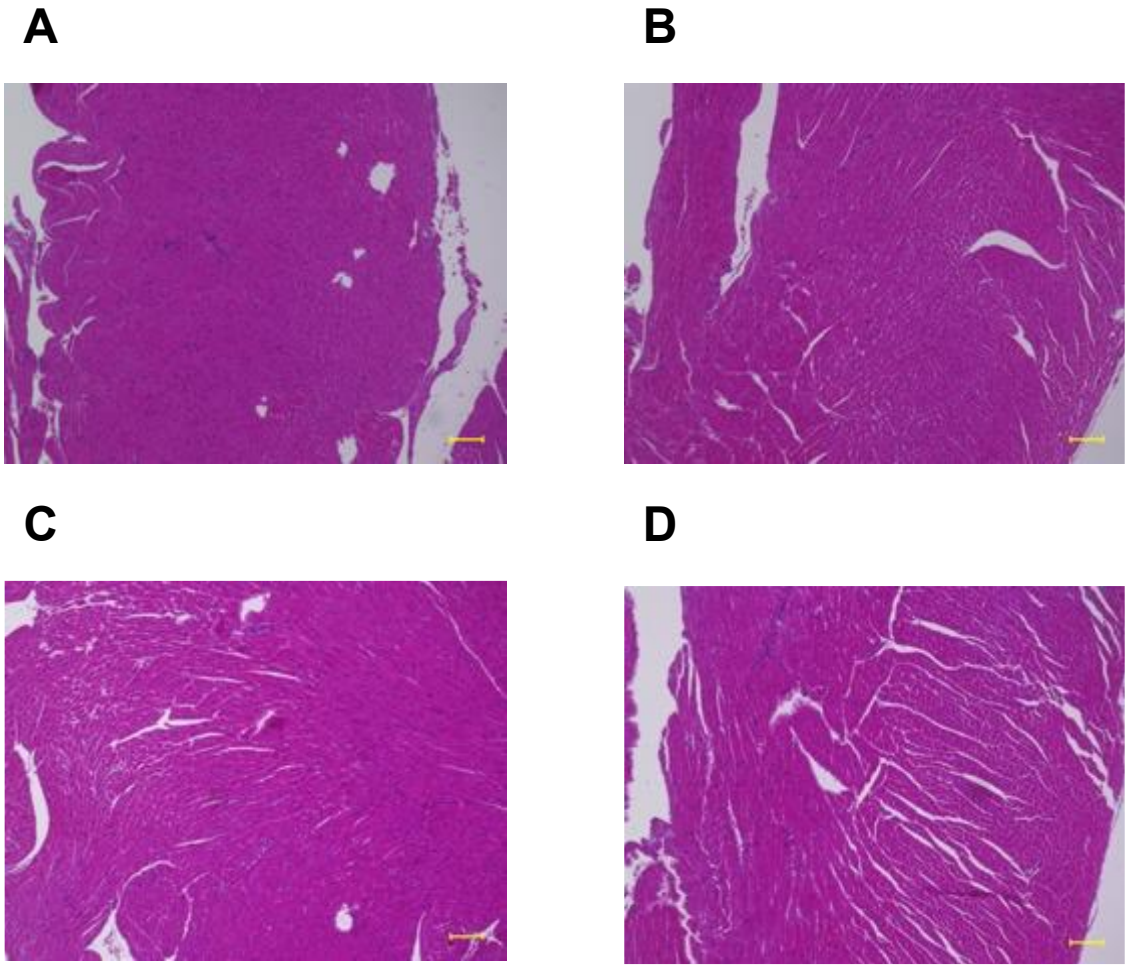

Figure 16. Histological images of hearts from mice treated with 3-CVBs.

H-E staining of hearts isolated from mice treated with vehicle control (A), WT-CVB (B), 3a-CVB (C), and 3c-CVB (D) two days after inoculation. Magnification: 10×. Scale bars, 100 μm.

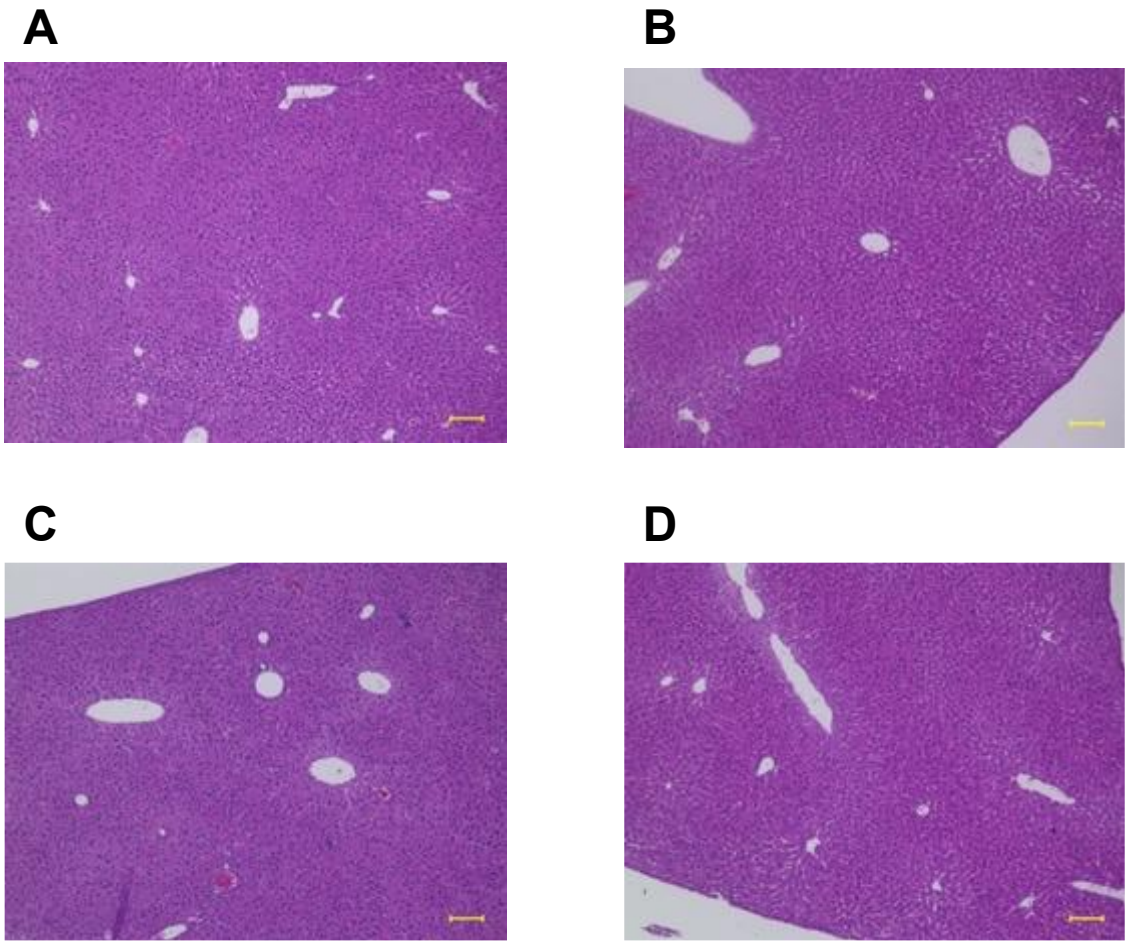

Figure 17. Histological images of livers from mice treated with 5-CVBs.

H-E staining of livers isolated from mice treated with vehicle control (A), WT-CVB (B), 5a-CVB (C), and 5c-CVB (D) two days after inoculation. Magnification: 10×. Scale bars, 100 μm.

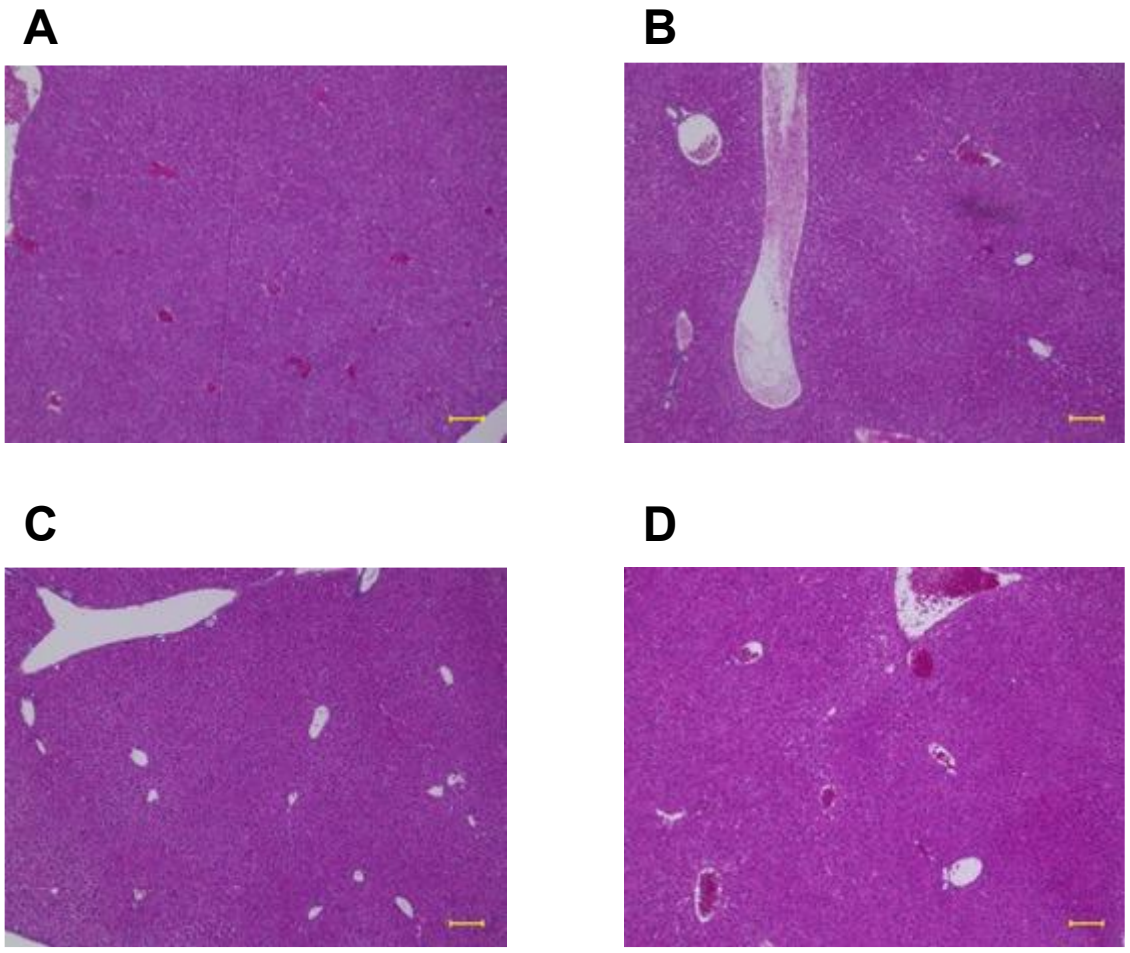

Figure 18. Histological images of livers from mice treated with 3-CVBs.

H-E staining of livers isolated from mice treated with vehicle control (A), WT-CVB (B), 3a-CVB (C), and 3c-CVB (D) two days after inoculation. Magnification: 10×. Scale bars, 100 μm.

Double insertion of miR-34aTs improves the safety of CVBs without diminishing their anti-tumor effect. To further improve the safety of 3a-CVB, we modified CVB3 to be more downregulated by miR-34a. For this purpose, we inserted four tandem miR-34aTs not only in the 3'UTR, but also in the 5'UTR of the CVB3 genome (53a-CVB), in order to increase the number of miR-34a–binding sites (Figure 19). We first compared the cytotoxicity of 53a-CVB in H1299 cells with that of 5a-CVB, 3a-CVB3, and WT-CVB. 53a-CVB3 exerted strong cytotoxicity in H1299 cells, like other miRT-CVBs, but less cytotoxicity than 5a-CVB and 3a-CVB in miR-34a–transfected H1299 cells (Figure 20). Although viral replication of miRT-CVBs was slower than that of WT-CVB, virus production of miRT-CVBs reached almost the same level as that of WT-CVB at 12 hrs or later in H1299 cells, and decreased virus production was observed in cells with a complementary combination of miRNAs and miRT-CVBs (Figure 21). 53a-CVB also killed other cell lines very efficiently, although HeLa cells were slightly more resistant to 53a-CVB than to WT-CVB (Figure 22). 53a-CVB also exerted significantly lower cytotoxicity than 5a-CVB3 and 3a-CVB in BEAS-2B cells (Figure 22). Furthermore, we observed an anti-tumor effect of 53a-CVB using H1299 cell–injected mice, and found that 53a-CVB induced complete tumor regression, similar to 5a-CVB, 3a-CVB, and WT-CVB (Figure 23), resulting in no tumor-associated death

(Figure 24). In contrast to WT-CVB– and 5a-CVB–treated mice, neither 3a-CVB– nor 53a-CVB–treated mice lost weight after starting the treatment (Figure 25).

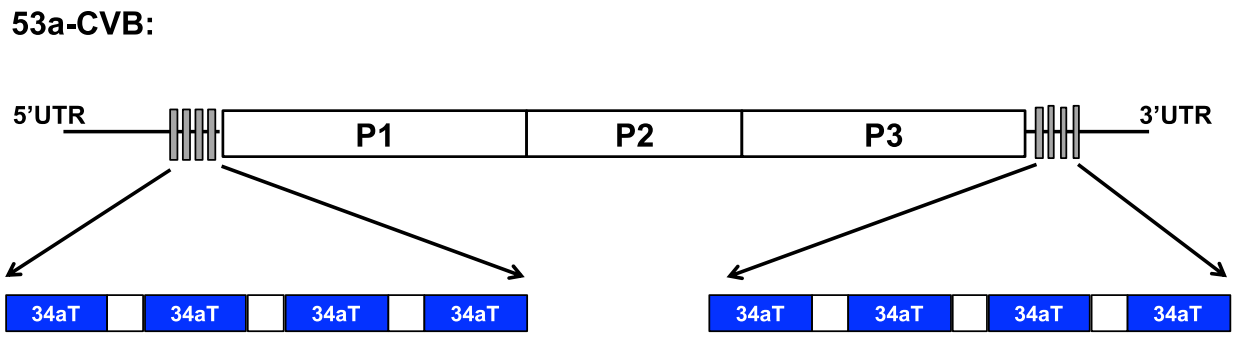

Figure 19. Schematic diagram of 53a-CVB.

Four tandem 34aT or 34cT constructed in both 5'UTR and 3'UTR of CVB3 genome.

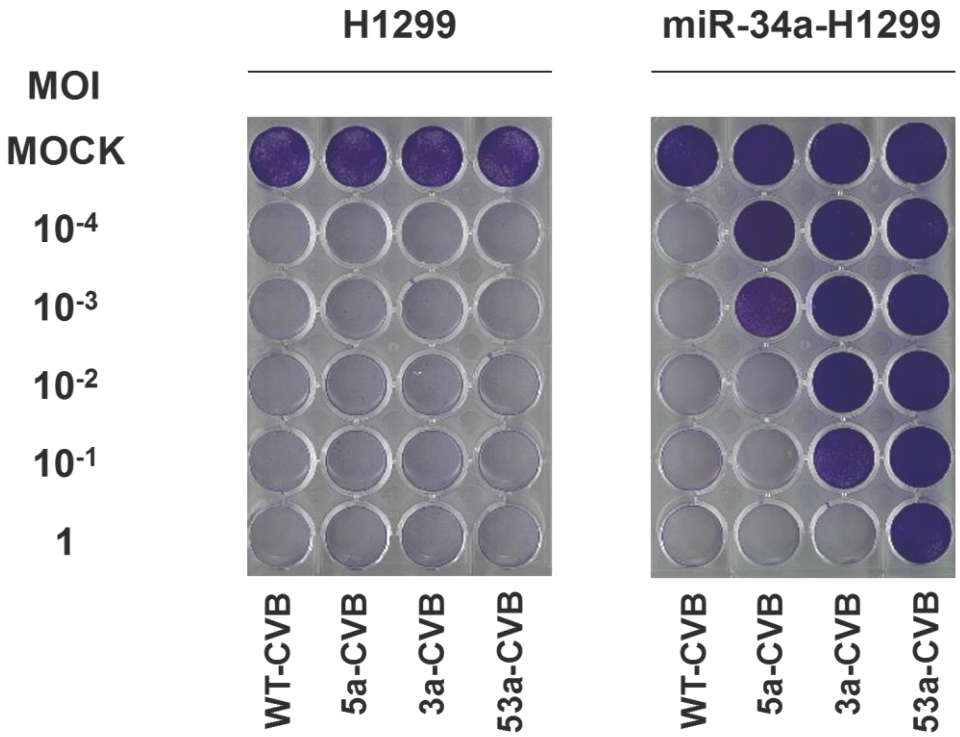

Figure 20. Reduced cytotoxicty of 53a-CVBs and in miR-34a mimic transfected cells.
Representative images of H1299 cells transfected with miR-34a mimics, followed by inoculation with indicated viruses at an MOI of 10^{-4} to 1. Cytotoxicity of each virus was determined by crystal violet staining 72 hrs after infection. All experiments were repeated at least three times.

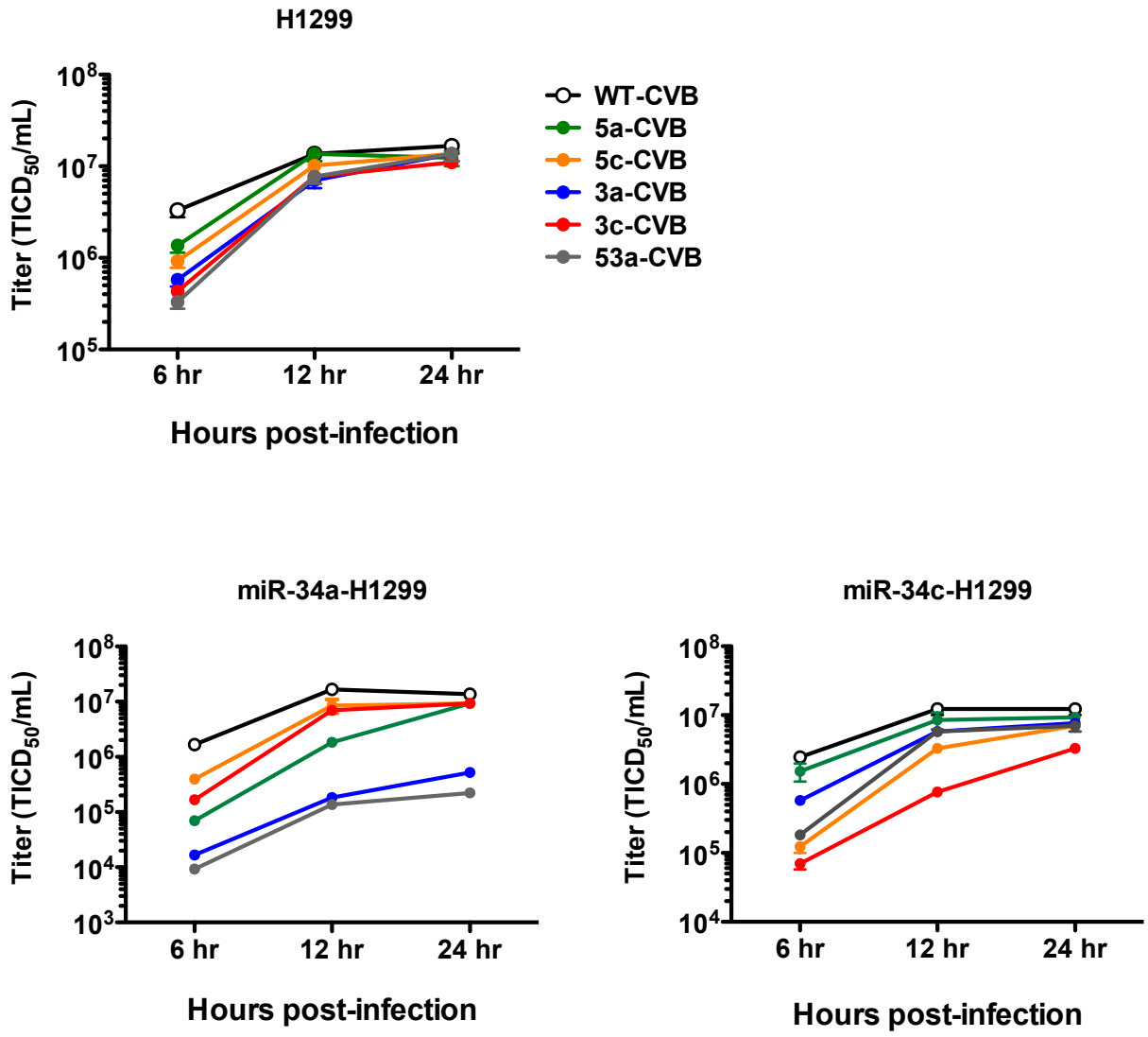

Figure 21. Reduced replication of miRT-CVBs in mimics-transfected cells.

Replication kinetics of miRT-CVBs were evaluated using single-step growth curve analysis (MOI = 3) in H1299 cells transfected with miR-34a mimics (miR-34a-H1299) or miR-34c mimics (miR-34c-H1299). Data are represented as mean virus titer ± SD.

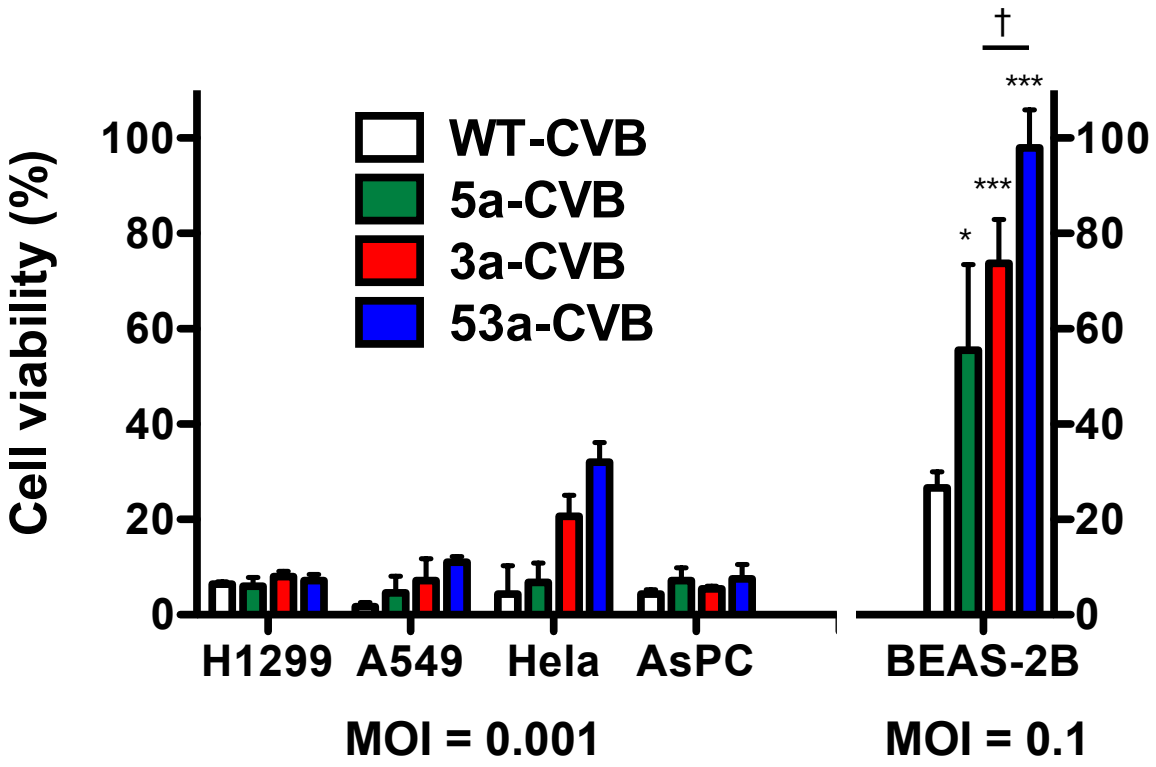

Figure 22. Viability of cancer cell lines and BEAS-2B cells infected with 53a-CVBs.

Cell viability of cancer cell lines and BEAS-2B cells was determined by MTS assay 72 hrs after inoculation with the indicated viruses. Data represent means ± SD of relative viable cell number vs. un-infected cell number from triplicate assays. *, $p < 0.05$; ***, $p < 0.001$ vs. CVB3-WT (t-test). †, $p < 0.05$ CVB3-53A vs. CVB3-3A (t-test).

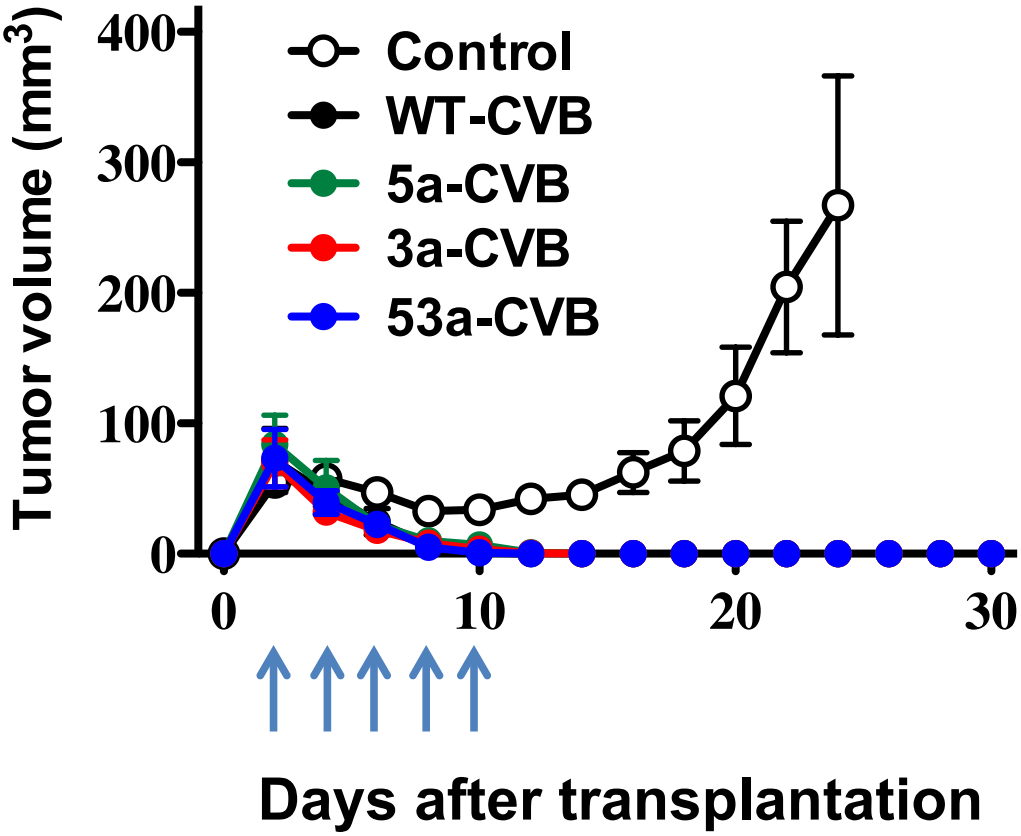

Figure 23. Tumor growth of H1299 xenografts treated with 53a-CVB.

BALB/c nude mice received s.c. transplantation of 5×10^6 H1299 cells. Arrows indicate the timing of five doses (5×10^6 $TCID_{50}$) of i.t. injection of indicated viruses or 5a-CVB, 3a-CVB, 53a-CVB, WT-CVB, and vehicle control. Tumor volume was measured every 2 days. Data represent means ± SD of each group.

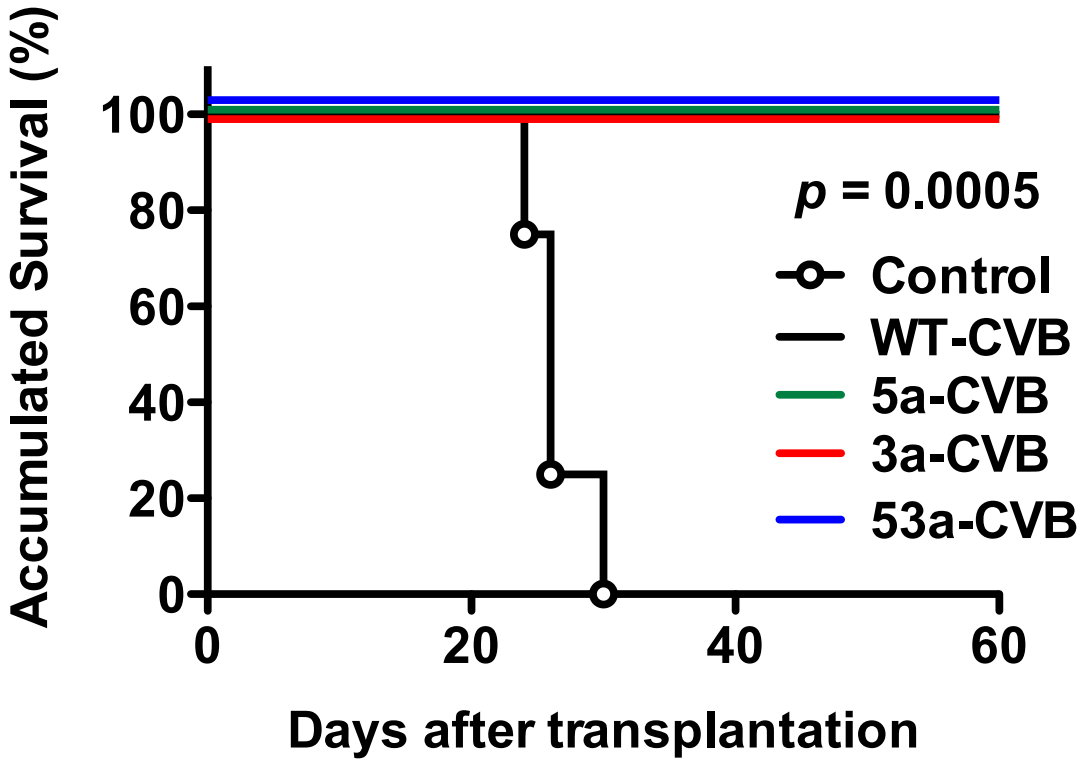

Figure 24. Overall survival of H1299-transplaned mice treated with 53a-CVB.

Kaplan–Meier survival curves of mice treated with indicated CVBs are shown. Each group consists of five mice. *p*, statistical difference between the control group and each virus-treated group calculated by log–rank test.

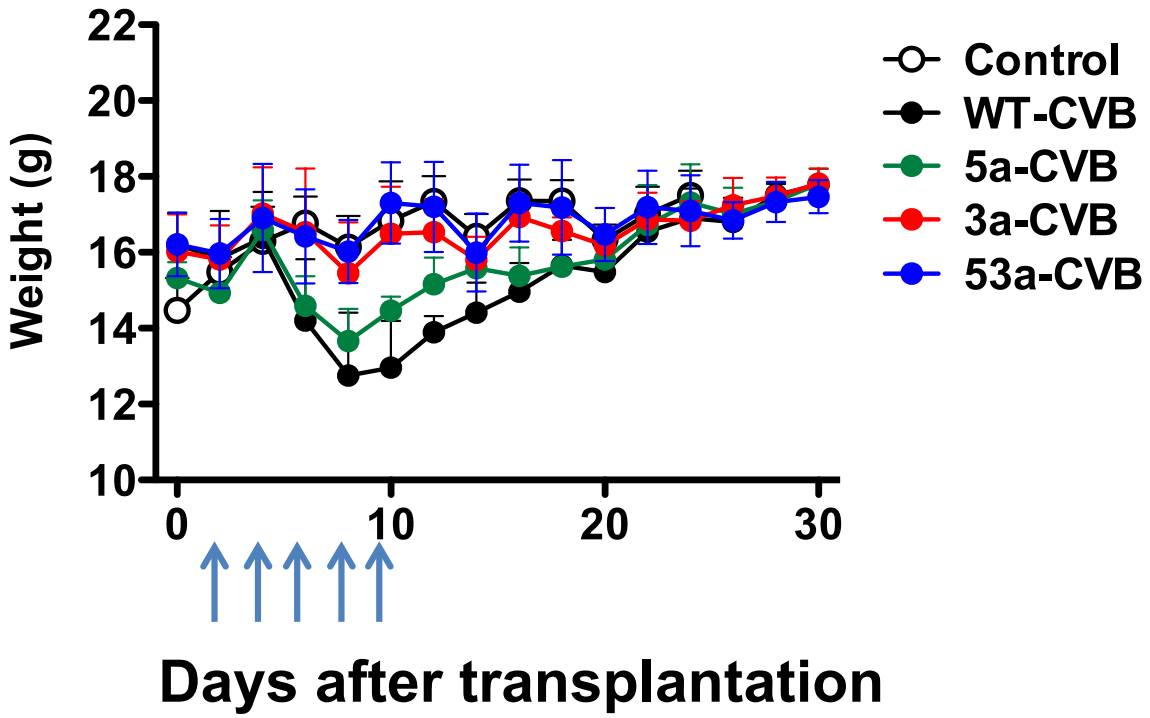

Figure 25. Body weight of H1299-transplanted mice treated with 53a-CVB.

Body weight of mice treated with indicated CVBs was measured every 2 days. Data represent means ± SD. Each group consists of four or five mice.

Aberrantly activated oncogenic pathways defeat miRT-mediated inhibition of CVB3 replication.

As shown in Figure 22, although miR-34a was expressed at higher levels in A549 and Hela cells than in normal bronchial BEAS-2B cells, 53a-CVB as well as 5a- or 3a-CVB exerted stronger cytotoxicity in these tumor cells at much lower titers than in non-tumor cells. Since CVB3 replication is dependent on signaling pathways such as PI3K/Akt and MAP/ERK/MEK, which are aberrantly activated in tumor cells (*27, 49*), we hypothesized that those activated pathways would overcome miR-34a-downregulated CVB3 replication in tumor cells. To demonstrate this hypothesis, we examined the inhibited effect of those pathways on the cytotoxicity of miRT-CVBs in cancer cell lines. While a PI3K inhibitor LY294002 or MEK inhibitor PD0325901 decreased the cytotoxicity of WT-CVB to some extent in A549 cells, these inhibitors further decreased the cytotoxicity of miR-34aT–CVBs, particularly 53a-CVB (Figure 26), which supported our hypothesis. In contrast, a reduction in cytotoxicity by those inhibitors was independent of the type of CVBs in AsPC cells expressing a very low level of miR-34a. This result further suggests that miR-34a-induced inhibition of miR-34aT-CVB replication could be overridden by aberrantly activated PI3K/Akt and/or MAP/ERK/MEK pathways in tumor cells.

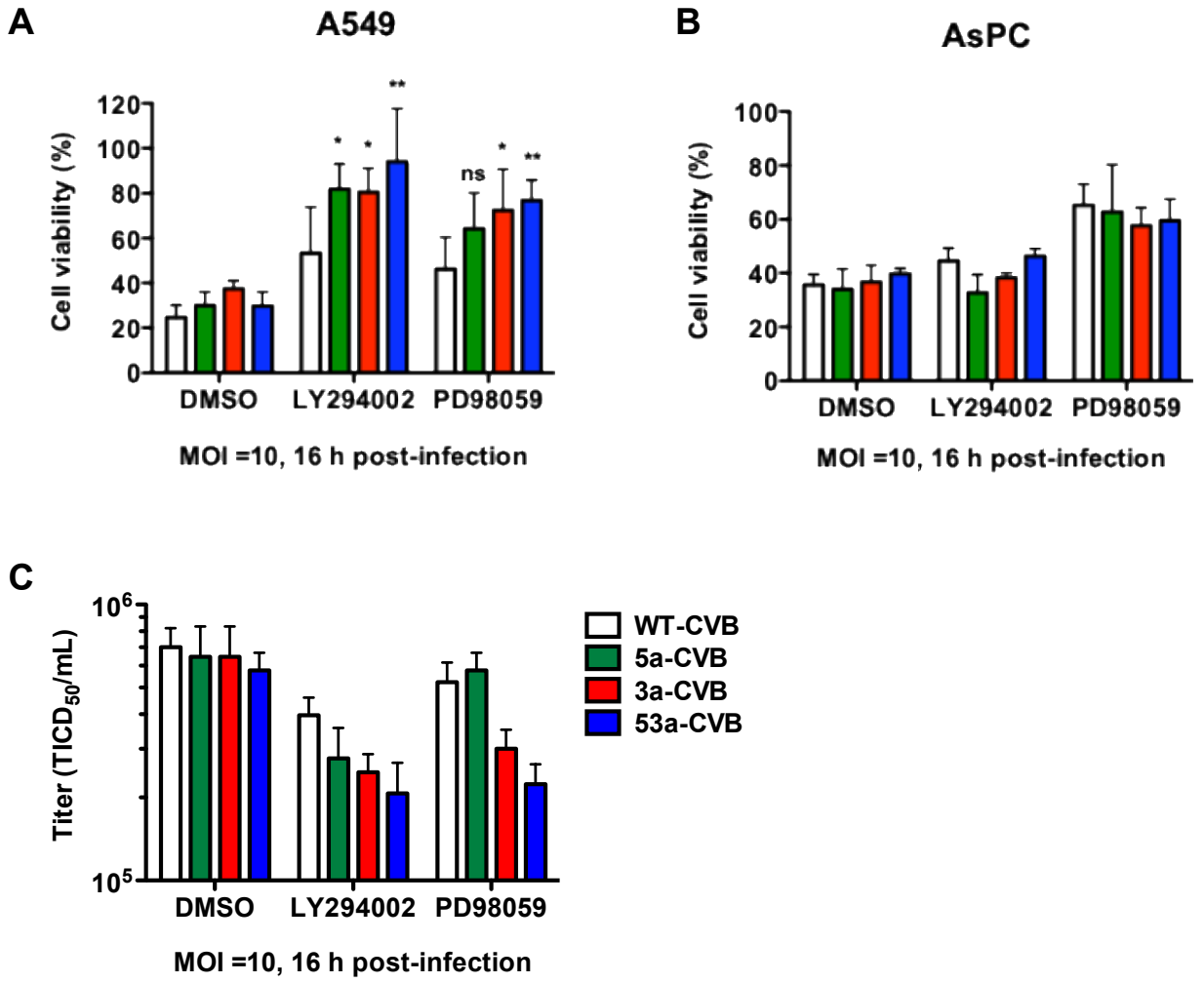

Figure 26. Attenuated cytotoxicity of miR34T-CVBs in miR34a-high A549 cells by treatment with PI3K inhibitor LY294002 or MEK inhibitor PD98059.

A549 cells (miR34a-high) (A) and AsPC cells (miR34a-low) (B) were treated with 10 μM LY294022, 10 μM PD0335901 or DMSO for 1 hour followed by inoculation with indicated CVBs. 16 hours later, MTS assay was performed to determine living cells. *, $p < 0.05$; **, $p < 0.01$ vs. WT-CVB (t-test) and there is no statistically significant difference between each group by ANOVA in AsPC cells. (C) Supernatants from A549 cells were collected and a viral titer was determined.

Extremely low toxicity of 53a-CVB in tumor mouse models. To confirm the safety of 53a-CVB *in vivo*, we evaluated organ injury by performing blood biochemistry test and pathological examination in mice injected with H1299 cells. As in previous experiments (Figure 11 -13), although no CVBs increased serum BUN or T-bil levels (Figure 27), WT-CVB and 5a-CVB significantly increased serum AST, ALT, LDH, and amylase, whereas 3a-CVB induced mild elevation of ALT (Figure 28). By contrast, there was no significant elevation of these enzymes, including ALT, in mice treated with 53a-CVB, suggesting almost complete elimination of CVB-induced organ toxicity (Figure 5A). Moreover, a pathological study revealed that the 53a-CVB–treated mice did not have pancreatitis, in contrast to mice treated with the other miRT-CVBs (Figure 29). Moreover, there were no pathological changes in the heart or liver in mice treated with 53a-CVB, as in mice treated with other CVBs (Figure 30, 31).

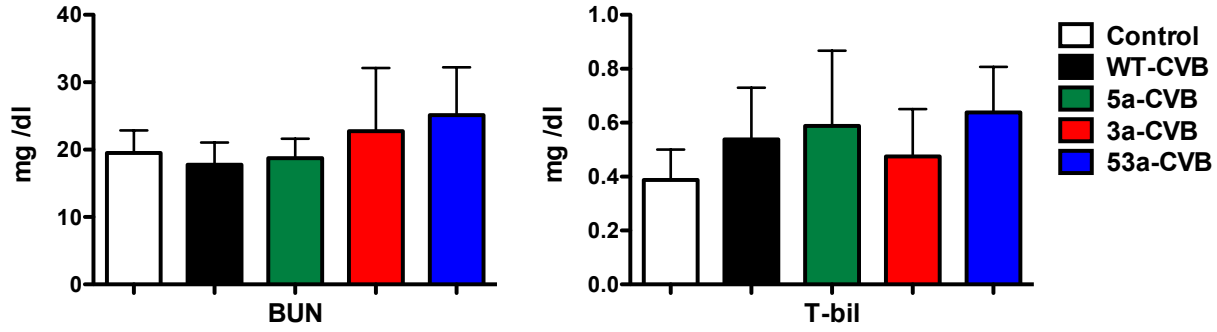

Figure 27. Serum levels of BUN and T-bil in tumor-harboring mice treated with 53a- or other CVBs.

BALB/c nude mice were injected with indicated CVBs (5×10^6 $TCID_{50}$) or vehicle controls two days after H1299 cell transplantation. Mouse blood samples were collected two days after infection, followed by immediate analysis of serum BUN and T-bil. Results are shown for mice treated with indicated CVBs or vehicle control. Data represent means ± SD of eight or nine mice in each group. There are no statistically significant difference between each group by ANOVA.

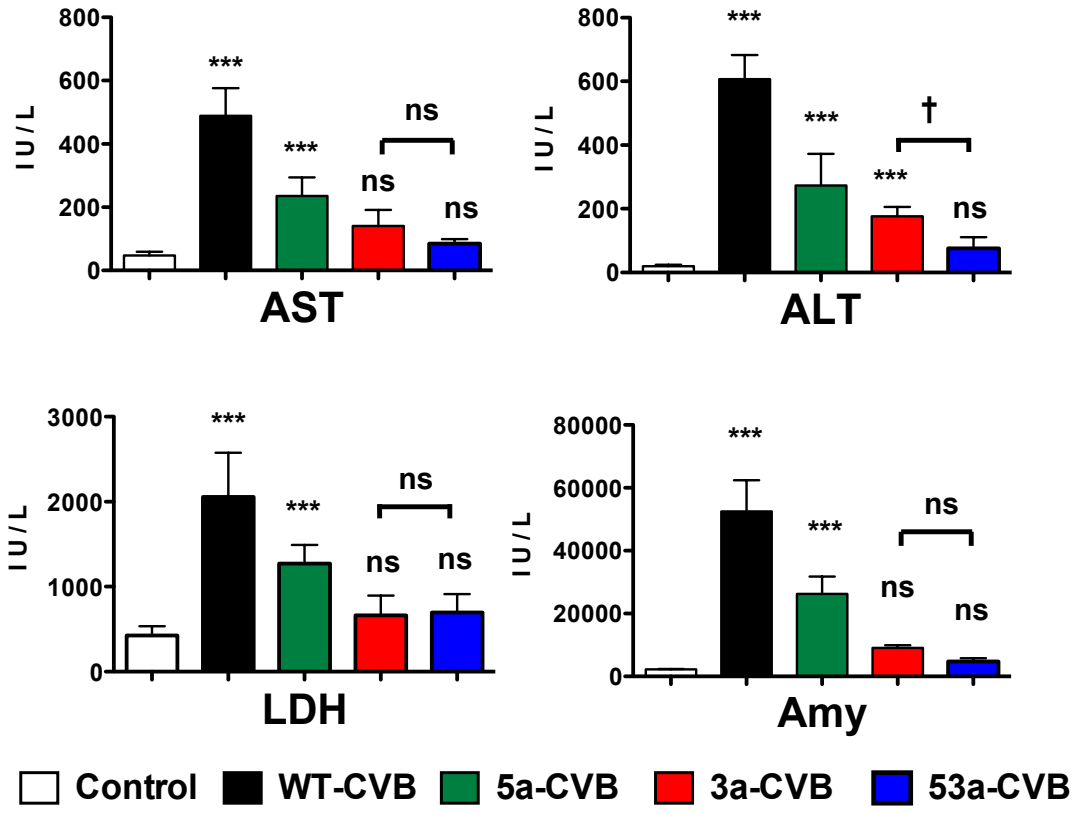

Figure 28. Blood biochemistry test results of tumor-harboring mice treated with 53a- or other CVBs. BALB/c nude mice were injected with indicated CVBs (5×10^6 $TCID_{50}$) or vehicle controls two days after H1299 cell transplantation. Mouse blood samples were collected two days after CVB injectin, followed by immediate analysis of serum ALT, AST, LDH, and amylase. Data represent means ± SD (n = 8 /group). ***, $p < 0.001$ vs. control mice (Tukey's test). †, $p < 0.05$ 53a-CVB group vs. 3a-CVB3 group (Tukey's test).

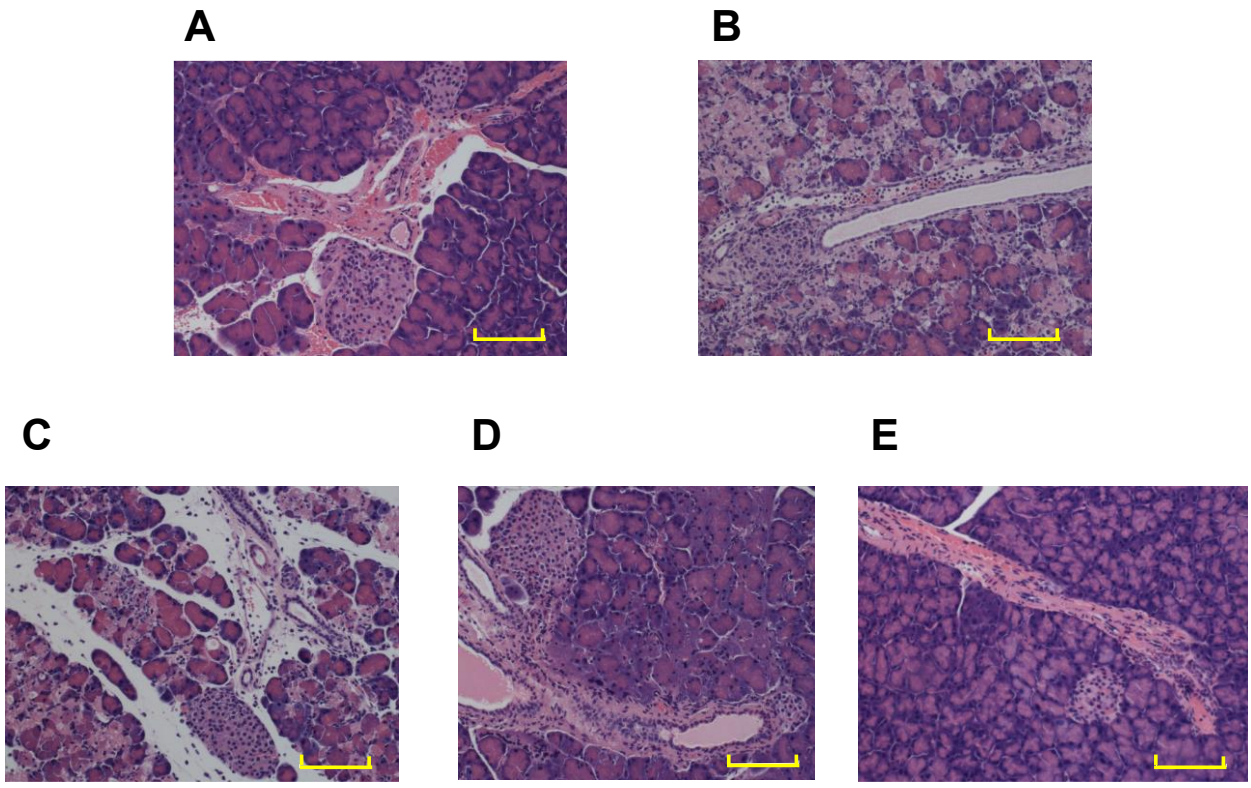

Figure 29. Pathological examination of pancreas from tumor-harboring mice treated with 53a- or other CVBs.

Pathological images of pancreas two days after injection of indicated CVBs. Vehicle control (A), WT-CVB (B), 5a-CVB (C), 3a-CVB (D), and 53a-CVB (E). Magnification: 10× + 2× zoom. Scale bar, 100 μm. All experiments were repeated twice.

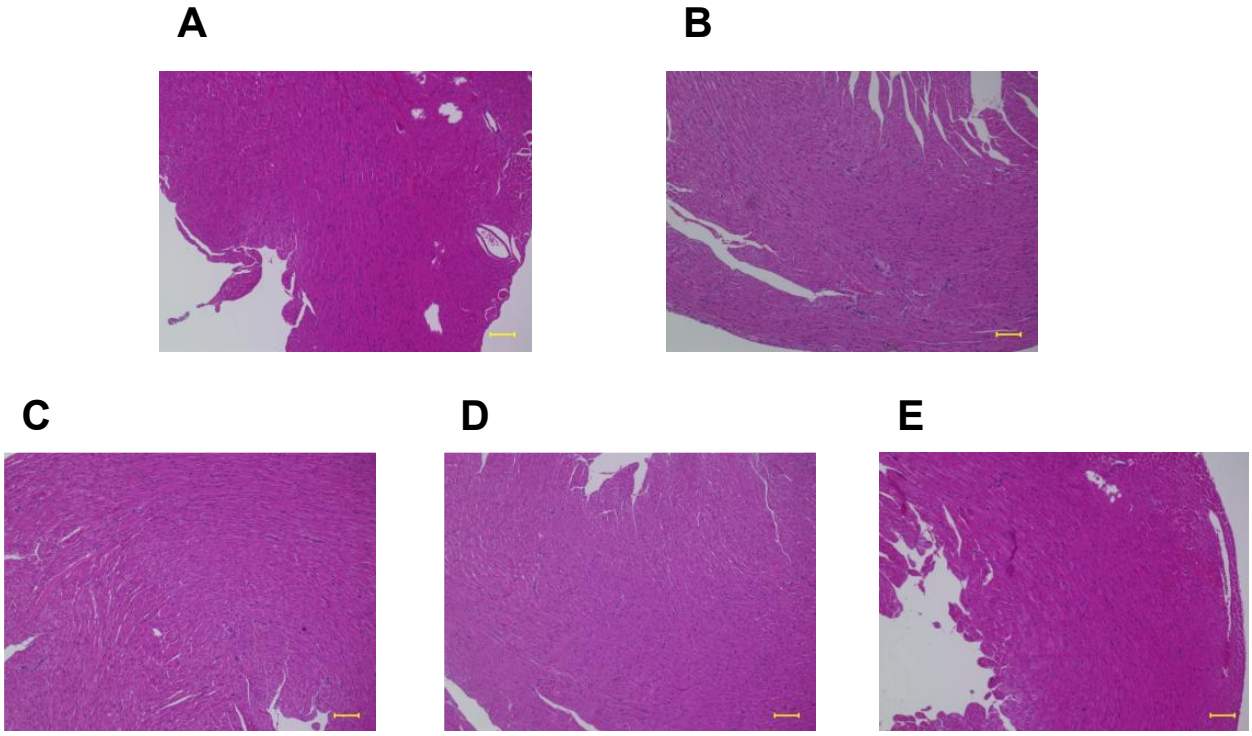

Figure 30. Histological images of hearts from tumor-harboring mice treated with 53a- or other CVBs.

H-E staining images of hearts two days after injection of indicated CVBs. Vehicle control (A), WT-CVB (B), 5a-CVB (C), 3a-CVB (D), and 53a-CVB (E). Magnification: 10×. Scale bars, 100 μm.

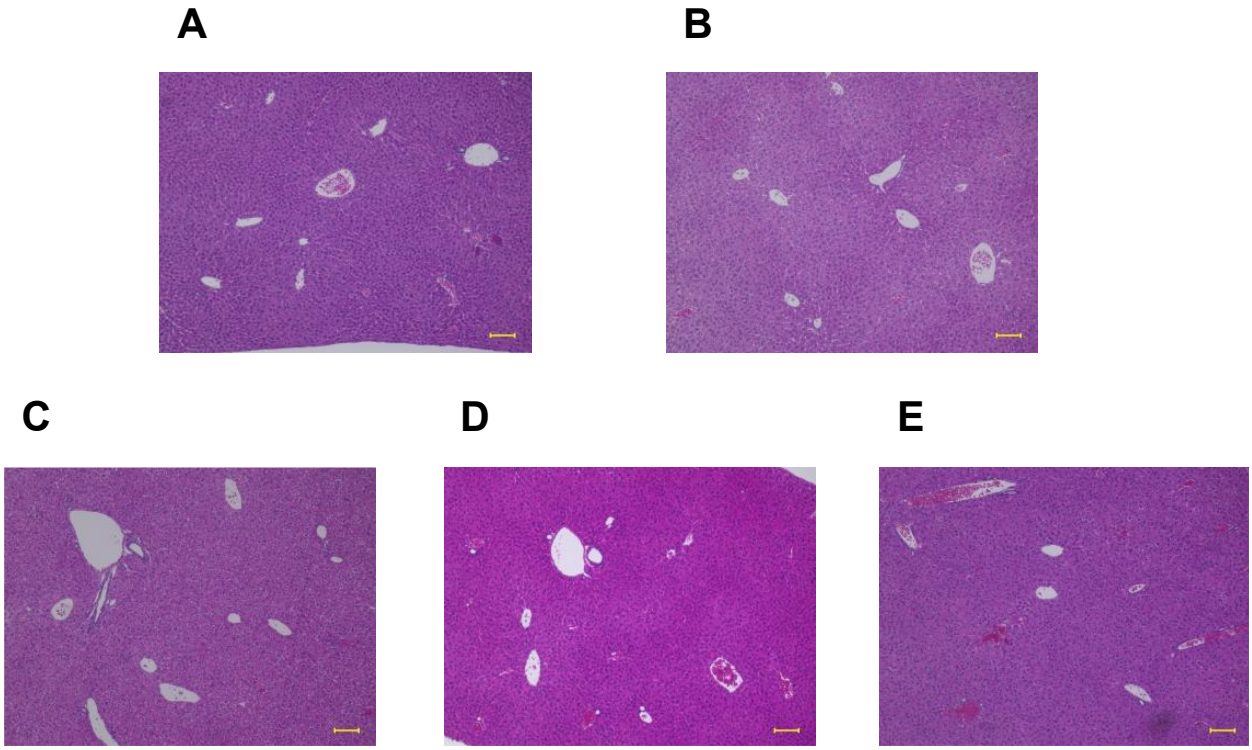

Figure 31. Histological images of livers from tumor-harboring mice treated with 53a- or other CVBs.

H-E staining images of hearts two days after injection of indicated CVBs. Vehicle control (A), WT-CVB (B), 5a-CVB (C), 3a-CVB (D), and 53a-CVB (E). Magnification: 10×. Scale bars, 100 μm.

Biodistribution of CVBs in tumor-harboring mice. To determine proliferation site of CVBs in the mouse xenograft model of human lung cancer, we examined copy numbers of CVB genome in each mouse organ. Mouse tumors or organs were collected two days after CVB injection, and the virus copy numbers were determined by RT-qPCR (Figure 32A). In mice treated with WT-CVB, pancreas was the top organ of viral copy numbers besides tumors, followed by spleen, heart, and lung. We also detected about 1/100 of virus in all other organs. Of note is that in 53a-CVB-treated mice, pancreas showed about 1/100 virus copy numbers than that in WT-CVB-treated mice and the other organs did not show detectable viruses, while tumors of both mice had almost same virus load. Since WT-CVB-treated mice but not 53a-CVB-treated mice showed detectable virus load in all organs despite no obvious signs of tissue damages in all organs except pancreas, I speculated that the virus detected in those organs could result from high virus load in their circulating blood. To address this question, I examined virus load of mouse serum and found that the serum virus load of WT-CVB-treated mice was 10- fold higher than that of 53a-CVB-treated mice (Figure 32B), suggesting that in WT-CVB-treated mice, pancreas was a virus reservoir providing viruses to circulating blood, and the high circulating virus load resulted in detectable amount of viruses in the other organs. These data were consistent with the maintained anti-tumor effect and very low

toxicity of 53a-CVB, indicating that 53a-CVB is an excellent OV with the highest efficacy and safety.

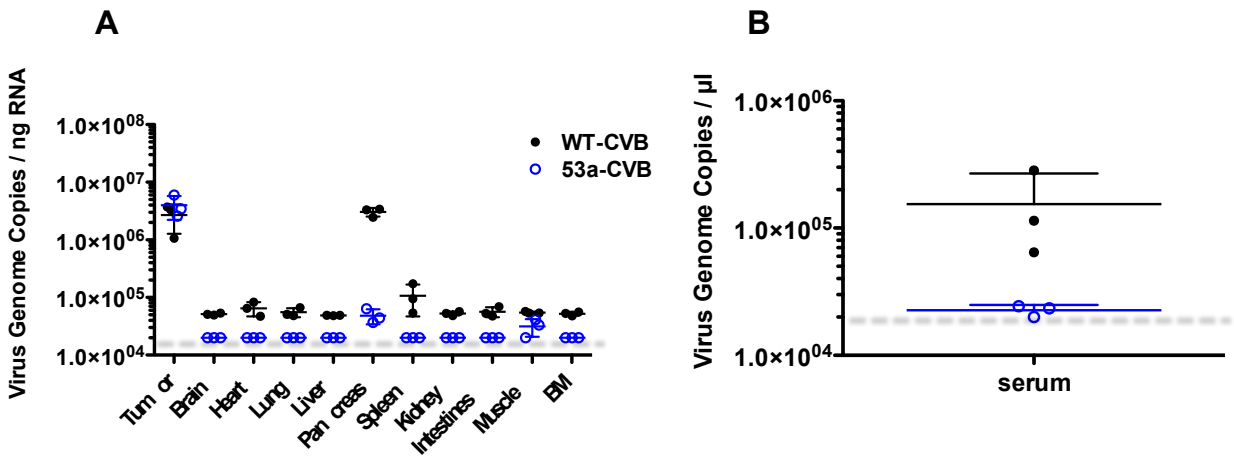

Figure 32. Biodistribution of CVBs in tumor-harboring mice treated with WT- or 53a-CVB. H1299 cells (5×10^6) were transplanted s.c. into BALB/c nude mice, and then the indicated viruses were injected with 5×10^6 $TCID_{50}$ two days after transplantation. Mouse organs (A) and serum (B) were collected two days after CVB injection, and the copy numbers of virus genome were quantified by RT-qPCR. The limit of detection is indicated by the dashed line (2×10^4 copies of virus RNA per ng). Data represent means ± SD of triplicated experiments.

No obvious toxicity of 53a-CVB in an immunocompetent mouse model of lung cancer. To address if any immunogenic response against CVBs could induce an adverse effect *in vivo*, we evaluated the toxicity of CVBs in syngeneic tumor transplantation models. C57BL/6J mice bearing subcutaneous tumors of mouse lung cancer TC-1 cells, which susceptible to CVB3 (Figure 33), received an i.t. injection of WT-, 5a-, 3a- or 53a-CVB. After 48 hrs, blood and organs were collected from those mice, and there were very similar findings to that of nude mouse xenograft models. This result further indicated that 53a-CVB also has extremely low toxicity in immunocompetent mice (Figure 34, 35).

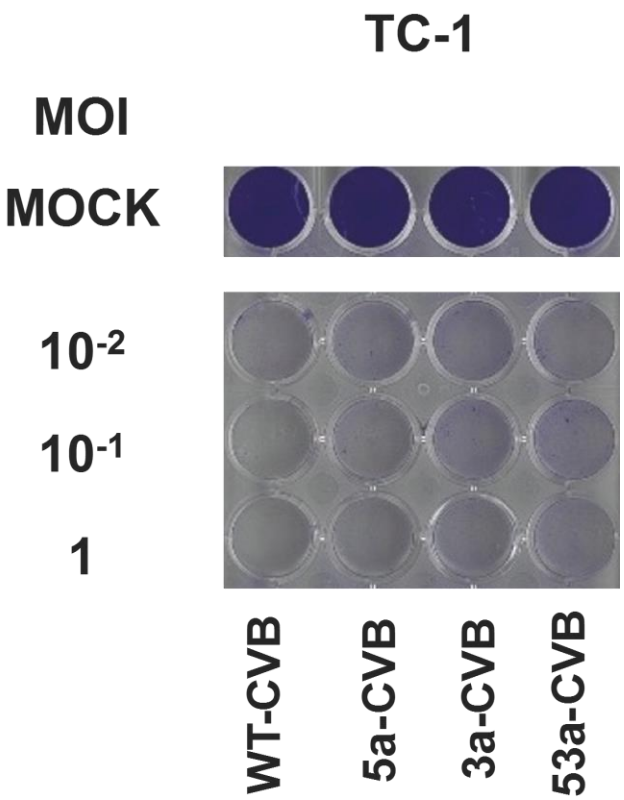

Figure 33. *In vitro* Cytotoxicity of miRT-CVBs in mouse lung cancer TC-1 cells.
Representative images of mouse lung cancer TC-1 cells inoculated with indicated viruses at an MOI of 10^{-2} to 1. The cytotoxicity of each virus was determined at 72 hrs post-infection.

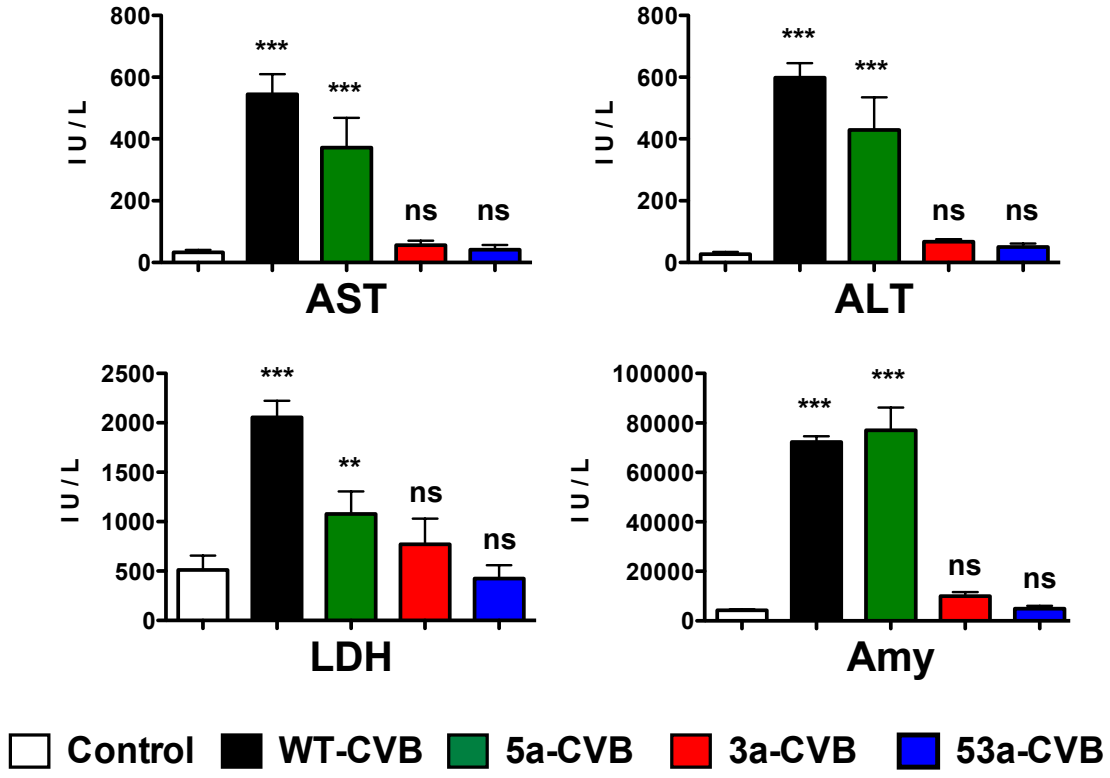

Figure 34. Blood biochemistry test results of syngeneic tumor-harboring immunocompetent mice treated with 53a- or other CVBs.

C57BL/6J mice were injected with indicated CVBs (5×10^6 $TCID_{50}$) or vehicle controls two days after mouse lung cancer TC-1 cell transplantation. (tumor size reached a diameter of 0.5 cm). Mouse blood samples were collected two days after CVB injection, followed by immediate analysis of serum ALT, AST, LDH, and amylase. Data represent means ± SD (n = 4/group). **, $p < 0.005$; ***, $p < 0.001$ vs. control group (Tukey's test).

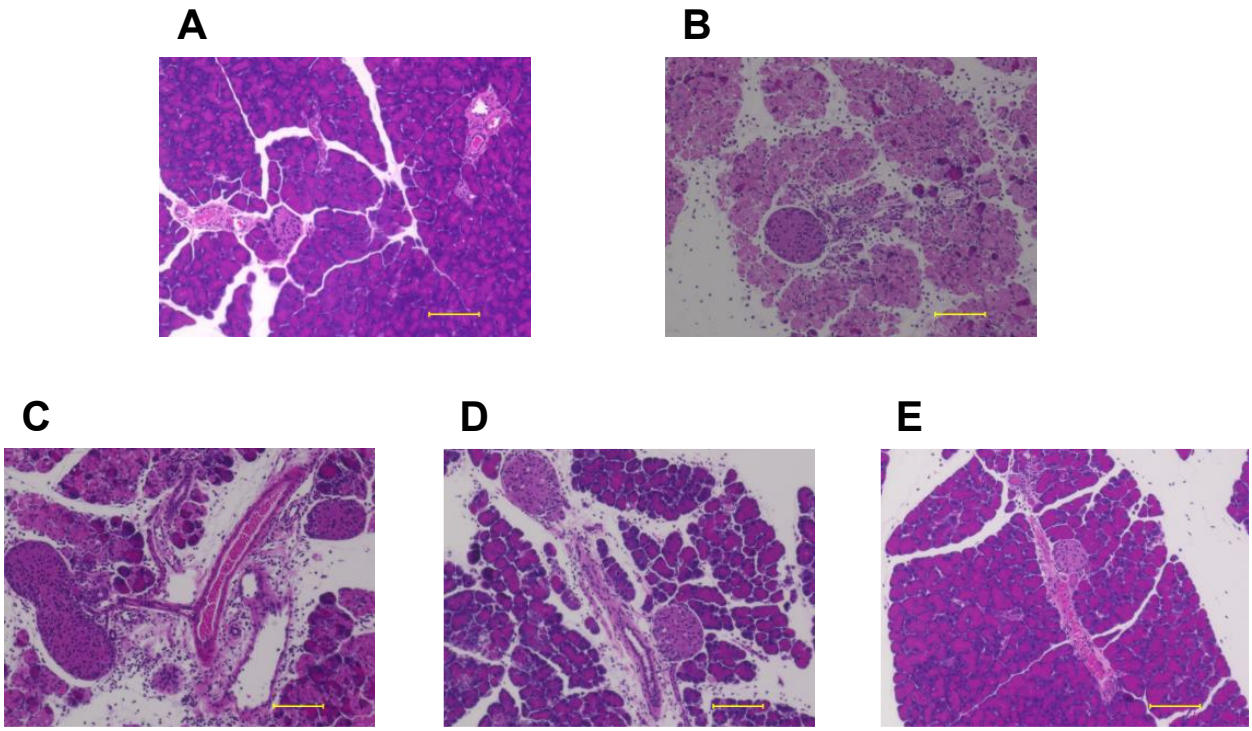

Figure 35. Pathological examination of pancreas from tumor-harboring C57BL/6 mice treated with 53a- or other CVBs.

Pathological images of pancreas two days after injection of CVBs. Vehicle control (A), WT-CVB (B), 5a-CVB (C), 3a-CVB (D), and 53a-CVB (E). Magnification: 20×. Scale bar, 100 μm.

Discussion

OVs are considered to be promising tools for cancer treatment, even for patients with disease that is resistant or refractory to chemotherapies or radiotherapies (*12*). RNA viruses seem to be a safer agent, because their replication occurs in cytoplasm and this process skips integration of viral genome into host genome, avoiding the risk of cellular mutagenesis. Among RNA viruses, CVA21 (CAVATAK^{TM}) is one of the most studied oncolytic RNA enteroviruses. Since CVB3 and CVA21 belong to the same enterovirus species, they perform same life cycle as well as antitumor activities. Due to their different receptors, CVA21 mainly binds to ICAM-1 while CVB3 mainly binds to CAR, they prosses different cell tropism, target of cancer, and pathogenicity. By now, Phase I trials of CVA21 against melanoma, breast cancer, NSCLC, prostate cancer, and head and neck cancer have been reported. These results showed that CVA21 was well-tolerated, with an increased number of infiltrating immune cells in tumor cells. The completed Phase II trial (NCT01227551) were designed to evaluate the efficacy of intratumoral CVA21 in 57 patients suffered from late-stage melanoma. The ORR assessed by irRECIST was 28.1% with >6 months durable response rate of 21.1%. Although no CVA21-induced death was observed, there was 19.3% (11/57) of serious adverse events, and 94.74% (54/57) of other adverse events in this study. Another Phase II

trial (NCT01636882) was proceed in 16 patients with late-stage melanoma to evaluate the safety of CVA21, and 6.25% (1/16) of all-cause mortality, 12.5 % (2/16) of serious adverse events, and 81.25% (13/16) of other adverse events were observed. Additionally, as CVA21 is a natural OV, the potential onset of upper respiratory symptoms still remains to be heeded (*50*). These problems would be overcome by using novel OVs including 53a-CVB.

In a previous study, our lab showed that CVB3 exerts a strong anti-tumor effect in a wide variety of tumors due to the broad expression of its receptors and its rapid replication in tumor cells (*1*). However, non-negligible toxicities were observed, particularly in pancreases, during the further characterization of WT-CVB for the purpose of clinical translation. Although WT-CVB did not cause death in NSCLC xenograft mice, those toxicities must be eliminated in order for CVB3-based OV to be used in the clinic. To this end, I adopted a gene expression regulation method using miRNA.

To date, the target sequences of let-7 miRNA family members, which are widely expressed in normal tissues, have been used to reduce toxicity of OVs in normal tissues. Insertion of the let-7 targets in OVs, however, often decreases not only normal tissue toxicity but also anti-tumor activity due to the extensive overlap in target sequences among its various family members (*51*). Therefore,

I tried to find other miRNA-regulating systems with stronger on-target effects and milder off-target effects. miR-34a, which is downregulated in various cancers, inhibits tumor growth in many types of cancers *in vitro* and *in vivo* including NSCLC (*52-58*). Consistent with a previous report (*40*), I observed generally higher expression of miR-34a and miR-34c in normal tissues than in cancer cells (Figure 1,2). Conveniently, in contrast to let-7, the miR-34 family consists of only three members, suggesting less interference among the family members. These findings encouraged us to develop safer and novel CVB3-based OVs by inserting miR-34 target sequences into the viral genome. As expected, insertion of miR-34aT and miR-34cT in CVB3s specifically reduced cytotoxicity in miR-34a– and miR-34c–transfected H1299 cells, respectively (Figure 5), and the miRT-CVBs showed very low toxicity in normal organs without losing the antitumor effect in mice harboring H1299 xenografts. Interestingly, despite the high expression of miR-34a, A549 and Hela cells were killed by miR-34aT–CVBs much more efficiently than normal bronchial BEAS-2B cells. The miR-34a–independent replication in cancer cells was suggested to be at least partially dependent on the PI3K/Akt and/or MAP/ERK/MEK pathways, which are aberrantly activated in many tumor cells (Figure 26). Therefore, miR-34aT–CVBs, particularly 53a-CVB, are thought to have antitumor effects in a wide variety of tumors, with low toxicity. Additionally, the slower

amplification of miRT-CVBs (Figure 21) did not affect the antitumor effect *in vitro* and *in vivo*, but could contribute to reduce the circulating virus (Figure 32B), resulting in less toxicity in normal organs.

When inserted into CVBs, miR-34aT was more effective than miR-34cT at reducing toxicities in normal tissues, possibly because all organs (including heart and pancreas, which are susceptible to CVB3) express miR-34a, whereas miR-34c is expressed only in lung and brain. Another possible reason for the difference in efficacy is the difference in miRNA target sites. Although miR-34a and miR-34c belong to the same seed family and share the same seed region (GGCAGTG) (*38*), the complementary sequences of the seed region and adjacent base of miR-34a is an 8mer-type site, whereas that of miR-34c is a 7mer-m8–type site (Figure 36). Although controversy persists on this issue, the 8mer-type site is thought to induce miRNA inhibition much more strongly than other types of sites, including 7mer-m8 (*59-62*). Therefore, the toxicities of 5a-CVB and 3a-CVB should be lower in miR-34a–expressing cells than those of 5c-CVB and 3c-CVB in miR-34c–expressing cells (Figure 5).

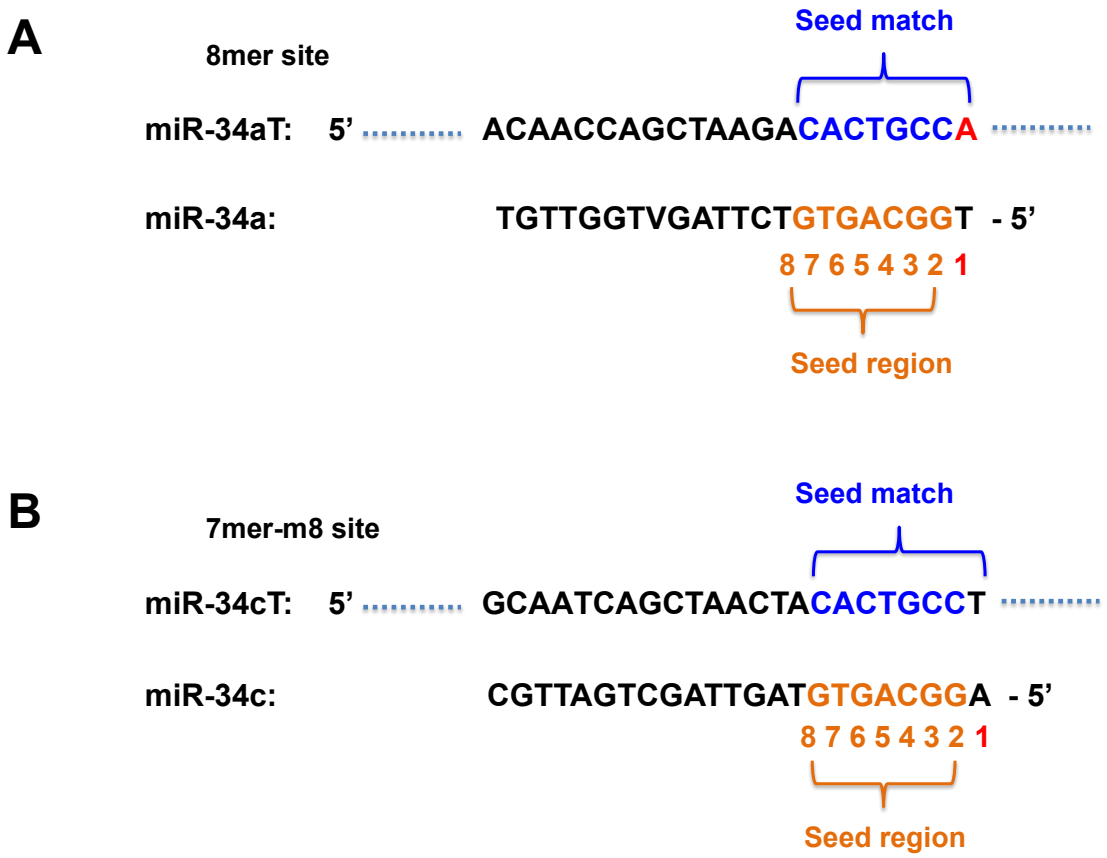

Figure 36. Nucleotide sequences of miR-34a, miR-34c, and their target sites.

A. miR-34a target site has seven contiguous Watson-Crick pairs complementary to the seed region (positions 2–8) of miR-34a, with an A at position 1.

B. miR-34c target site has a perfect match to the miRNA seed (positions 1-8).

On the other hand, the insertion site of miRT is another important factor to consider when seeking to suppress viral replication while maintaining oncolytic activity. Previously, the 5'UTR (*45, 63, 64*) and 3'UTR (*33, 35*) of CVB3 tolerate sequence insertion, although the core sequence of the internal ribosome entry site (IRES) was located at ntd 432–639 of CVB3 genome (5'UTR) (*65*), and in the 3'UTR, sites at ntd 7387 and ntd 7359–7360 do not tolerate sequence insertion (*45*). Thus, we avoided those sensitive sites for the purpose of miR-34aT and miR-34cT insertion. As expected, we could successfully insert miRTs into the 5'UTR, immediately upstream of the start codon, and into the 3'UTR at ntd 7,305, without losing anti-tumor effect of the original CVB3. We also found that 3-CVBs exhibited significantly lower pathogenicity than 5-CVBs (Figure 11 -13). Although we have not yet determined the reason, it seems that the effects of miRNAs are dependent on the locations of their target sequences. Several experimental (*60, 66-68*) and computational (*69, 70*) studies reported that a miRNA can inhibit a mRNA more efficiently when the target sequence is in the 3'UTR than in the 5'UTR or open reading frame. Although the mechanism underlying the reduced efficacy of miRNA in the 5'UTR remains unknown, it may involve detachment of RISC from the mRNA: RISC could easily be detached from miRTs when ribosomes bind to the 5'UTR at the beginning of translation, resulting in failure of miRNA regulation (*31*).

CVB3 is an RNA virus, viral genome mutation is known to occur with relatively high frequency because of the low fidelity of the viral RNA polymerase. In this study, 53a-CVB was serially passaged 10 times in H1299 cells, large deletions within the 3'UTR miRTs were observed. Our results were compatible with previous reported by Ruzi et al, who reported when miRNA-targeted viruses were serially passaged *in vitro* in the presence of the cognate miRNAs, large deletions within the insertion were observed (*35*).Multiple insertions of miRTs seemed to be a practical and easy strategy for improving the safety of 3a-CVB and avoiding the emergence of total deletion of a miRT insertion. Therefore, we engineered 53a-CVB by inserting 4 x miR-34aT sequences in both the 5' and 3'UTR. Even if deletion of miR-34aT occurred in one of the two miR-34aT sites in the 5' and 3'UTR, miR-34a was still accessible to the other miR-34aT site in the CVB genome, and virus replication would still be controllable by miR-34a. As expected, 53a-CVB exhibited an additive reduction in toxicity relative to 5a-CVB and 3a-CVB, with little toxicity in WT-CVB–sensitive organs such as the liver and pancreas, in mouse tumor models (Figure 28, 29). Moreover, 53a-CVB did not lose any of the antitumor activity of the original WT-CVB *in vitro* or *in vivo* (Figure 20-23), and could thus induce complete regression of tumors in all mice without obvious signs of adverse effects.

First of all, to perform human clinical trials of OVs, the toxicology assessment of these drugs using suitable animal model is required. The permissiveness of certain animal species to the candidate OV should be considered. Based on our preliminary studies BALB/c mouse was susceptible to CVB3 infection and replication and resulting pathological findings of infection could be reflected to human (*71*). Secondly, tumor-bearing xenograft or syngeneic animal models can be used to evaluate the safety of OVs. As the important difference between OVs and other traditional drugs is that OVs could replicate in tumor tissues, the viral level in a tumor-bearing model is significantly higher than in a tumor-free model. Pharmacology, biodistribution, and viral shedding of OVs in tumor-bearing models are significantly different from those in tumor-free model. Additionally, tumor-bearing models still have following limitations. I) The instability of tumor growth and viral replication in tumor would limit the assessment of the off-target toxicity of the virus. II) The assessment of immune response to the OV would also be limited because most of tumor-bearing models use immunodeficient mouse. III) Mouse would have reduced life span due to the tumor growth, resulting in limit availability for long-term safety evaluation. Because of this, tumor-free animal should also be used to evaluate the safety of OVs to complement the proof obtained from tumor-bearing models. Furthermore, the route of viral administration should mimic

the intended clinical trial as closely as possible. As intravenously (i.v.) administration of OVs would be limited by virus neutralizing antibody or hepatic clearance, intratumorally (i.t.) administration seems to be the most effective and safest route for OVs (*72*). Therefore, single-dose studies by i.t. administration were performed under clinically relevant conditions in tumor-bearing mice which allowed viral replication in patients.

In summary, the results of this study are considered to provide preclinical proof of principle that 53a-CVB was minimally toxic to normal tissues but maintained nearly full oncolytic activity in tumor, and is worth to be evaluated in the following second-stage toxicity study including i.v. toxicity studies.

According to the previous study, CVB could mainly cause acute pancreatitis, the level of amylase was increased in the early time points, and returned to normal on day 4 or 5 post-injection (*73, 74*). To better evaluate the virus-induced pathogenesis of miRT-CVBs and WT-CVB, the day 2 post-injection was chosen as an endpoint in this study.

Conclusion and Perspective

I successfully developed a potent and safe OV of 53a-CVB, by inserting miR-34aTs in both of 5'UTR and 3'UTR of WT-CVB. Although I demonstrated the minimal toxicity of 53a-CVB to

normal tissues without losing antitumor activities in the tumor-bearing models, two major important issues still remain to be addressed. First of all, to perform both stable and reproducible toxicity test, both of tumor-bearing mice models and tumor-free mice models should be used to evaluate the safety of 53a-CVB with 10 or 100 folds of dose, which have been used in tumor-bearing model, to complement the proof. Next, it is very important to set up the most appropriate duration for safety studies. To evaluate acute and chronic toxicities induced by virus, the observed period should be prolonged, and the clinical signs including physiological, biochemical, and histological consequences should be evaluated at multiple time points (day 0, 1, 3, 5, 7, 14, etc.).

Overall, our findings strongly suggested that 53a-CVB would be a promising OV that could be useful in the clinical setting due to its minimal toxicity and strong oncolytic effects.

References

1. S. Miyamoto *et al.*, Coxsackievirus B3 Is an Oncolytic Virus with Immunostimulatory Properties That Is Active against Lung Adenocarcinoma. *Cancer Research* **72**, 2609-2621 (2012).
2. F. f. t. P. o. C. Research., "Cancer Statistics in Japan, 2015," (March, 2016.).
3. S. N. Lester, K. Li, Toll-Like Receptors in Antiviral Innate Immunity. *Journal of Molecular Biology* **426**, 1246-1264 (2014).
4. S. B. Fleming, Viral Inhibition of the IFN-Induced JAK/STAT Signalling Pathway: Development of Live Attenuated Vaccines by Mutation of Viral-Encoded IFN-Antagonists. *Vaccines* **4**, (2016).
5. M. A. Garcia *et al.*, Impact of protein kinase PKR in cell biology: from antiviral to antiproliferative action. *Microbiology and Molecular Biology Reviews* **70**, 1032-+ (2006).
6. M. J. Clemens, Targets and mechanisms for the regulation of translation in malignant transformation. *Oncogene* **23**, 3180-3188 (2004).
7. Y. H. Huang, S. Goel, D. G. Duda, D. Fukumura, R. K. Jain, Vascular Normalization as an Emerging Strategy to Enhance Cancer Immunotherapy. *Cancer Research* **73**, 2943-2948 (2013).
8. C. J. Breitbach *et al.*, Targeting Tumor Vasculature With an Oncolytic Virus. *Molecular Therapy* **19**, 886-894 (2011).
9. M. T. Bejarano, J. R. Merchan, Targeting tumor vasculature through oncolytic virotherapy: recent advances. *Oncolytic Virotherapy* **4**, 169-181 (2015).
10. F. A. Angarita, S. A. Acuna, K. Ottolino-Perry, S. Zerhouni, J. A. McCart, Mounting a strategic offense: fighting tumor vasculature with oncolytic viruses. *Trends in Molecular Medicine* **19**, 378-392 (2013).
11. S. J. Ries, C. H. Brandts, Oncolytic viruses for the treatment of cancer: current strategies and clinical trials. *Drug Discovery Today* **9**, 759-768 (2004).
12. H. L. Kaufman, F. J. Kohlhapp, A. Zloza, Oncolytic viruses: a new class of immunotherapy drugs (vol 14, pg 642, 2015). *Nature Reviews Drug Discovery* **15**, (2016).
13. S. J. Russell, K. W. Peng, Oncolytic Virotherapy: A Contest between Apples and

Oranges. *Molecular Therapy* **25**, 1107-1116 (2017).

14. R. H. I. Andtbacka *et al.*, Talimogene Laherparepvec Improves Durable Response Rate in Patients With Advanced Melanoma. *Journal of Clinical Oncology* **33**, 2780-U2798 (2015).
15. K. Twumasi-Boateng, J. L. Pettigrew, Y. Y. E. Kwok, J. C. Bell, B. H. Nelson, Oncolytic viruses as engineering platforms for combination immunotherapy. *Nature Reviews Cancer* **18**, 419-432 (2018).
16. C. Heise *et al.*, Efficacy of a replication-selective adenovirus against ovarian carcinomatosis is dependent on tumor burden, viral replication and p53 status. *Gene Therapy* **7**, 1925-1929 (2000).
17. K. Fukuda *et al.*, E1A, E1B double-restricted adenovirus for oncolytic gene therapy of gallbladder cancer. *Cancer Research* **63**, 4434-4440 (2003).
18. M. A. Strassburg, THE GLOBAL ERADICATION OF SMALLPOX. *American Journal of Infection Control* **10**, 53-59 (1982).
19. G. L. Smith, A. Vanderplasschen, M. Law, The formation and function of extracellular enveloped vaccinia virus. *Journal of General Virology* **83**, 2915-2931 (2002).
20. B. He *et al.*, Suppression of the phenotype of gamma(1)34.5(-) herpes simplex virus-1: Failure of activated RNA-dependent protein kinase to shut off protein synthesis is associated with a deletion in the domain of the alpha 47 gene. *Journal of Virology* **71**, 6049-6054 (1997).
21. K. Fruh *et al.*, A VIRAL INHIBITOR OF PEPTIDE TRANSPORTERS FOR ANTIGEN PRESENTATION. *Nature* **375**, 415-418 (1995).
22. H. L. Kaufman, C. E. Ruby, T. Hughes, C. L. Slingluff, Jr., Current status of granulocyte-macrophage colony-stimulating factor in the immunotherapy of melanoma. *Journal for immunotherapy of cancer* **2**, 11-11 (2014).
23. T. J. Tuthill, E. Groppelli, J. M. Hogle, D. J. Rowlands, Picornaviruses. *Cell Entry by Non-Enveloped Viruses* **343**, 43-89 (2010).
24. L. van der Linden, K. C. Wolthers, F. J. M. van Kuppeveld, Replication and Inhibitors of Enteroviruses and Parechoviruses. *Viruses-Basel* **7**, 4529-4562 (2015).
25. D. R. Shafren, D. T. Williams, R. D. Barry, A decay-accelerating factor-binding

strain of coxsackievirus B3 requires the coxsackievirus-adenovirus receptor protein to mediate lytic infection of rhabdomyosarcoma cells. *Journal of Virology* **71**, 9844-9848 (1997).

26. K. M. Bedard, B. L. Semler, Regulation of picornavirus gene expression. *Microbes and Infection* **6**, 702-713 (2004).
27. F. S. Garmaroudi *et al.*, Coxsackievirus B3 replication and pathogenesis. *Future Microbiology* **10**, 629-652 (2015).
28. R. E. Rhoades, J. M. Tabor-Godwin, G. Tsueng, R. Feuer, Enterovirus infections of the central nervous system. *Virology* **411**, 288-305 (2011).
29. K. R. Spindler, T. H. Hsu, Viral disruption of the blood brain barrier. *Trends in Microbiology* **20**, 282-290 (2012).
30. V. Ambros, The functions of animal microRNAs. *Nature* **431**, 350-355 (2004).
31. D. P. Bartel, MicroRNAs: Genomics, biogenesis, mechanism, and function. *Cell* **116**, 281-297 (2004).
32. M. V. Iorio, C. M. Croce, microRNA involvement in human cancer. *Carcinogenesis* **33**, 1126-1133 (2012).
33. E. J. Kelly, E. M. Hadac, S. Greiner, S. J. Russell, Engineering microRNA responsiveness to decrease virus pathogenicity. *Nature Medicine* **14**, 1278-1283 (2008).
34. M. F. Leber *et al.*, MicroRNA-sensitive Oncolytic Measles Viruses for Cancer-specific Vector Tropism. *Molecular Therapy* **19**, 1097-1106 (2011).
35. A. J. Ruiz, E. M. Hadac, R. A. Nace, S. J. Russell, MicroRNA-Detargeted Mengovirus for Oncolytic Virotherapy. *Journal of Virology* **90**, 4078-4092 (2016).
36. M. Shayestehpour *et al.*, Targeting human breast cancer cells by an oncolytic adenovirus using microRNA-targeting strategy. *Virus Research* **240**, 207-214 (2017).
37. L. He *et al.*, A microRNA component of the p53 tumour suppressor network. *Nature* **447**, 1130-U1116 (2007).
38. M. Rokavec, H. H. Li, L. C. Jiang, H. Hermeking, The p53/miR-34 axis in development and disease. *Journal of Molecular Cell Biology* **6**, 214-230 (2014).
39. D. G. Zhang, J. N. Zheng, D. S. Pei, P53/microRNA-34-induced metabolic regulation: new opportunities in anticancer therapy. *Molecular Cancer* **13**,

(2014).

40. H. Hermeking, The miR-34 family in cancer and apoptosis. *Cell Death and Differentiation* **17**, 193-199 (2010).
41. R. P. Tomko, R. L. Xu, L. Philipson, HCAR and MCAR: The human and mouse cellular receptors for subgroup C adenoviruses and group B coxsackieviruses. *Proceedings of the National Academy of Sciences of the United States of America* **94**, 3352-3356 (1997).
42. C. B. Coyne, J. M. Bergelson, CAR: A virus receptor within the tight junction. *Advanced Drug Delivery Reviews* **57**, 869-882 (2005).
43. J. Y. Liu, S. M. Wang, I. C. Chen, C. K. Yu, C. C. Liu, Hepatic damage caused by coxsackievirus B3 is dependent on age-related tissue tropisms associated with the coxsackievirus-adenovirus receptor. *Pathogens and Disease* **68**, 52-60 (2013).
44. J. B. Rohll, D. H. Moon, D. J. Evans, J. W. Almond, THE 3'-UNTRANSLATED REGION OF PICORNAVIRUS RNA - FEATURES REQUIRED FOR EFFICIENT GENOME REPLICATION. *Journal of Virology* **69**, 7835-7844 (1995).
45. F. He *et al.*, Coxsackievirus B3 engineered to contain microRNA targets for muscle-specific microRNAs displays attenuated cardiotropic virulence in mice. *J Virol* **89**, 908-916 (2015).
46. B. D. Brown *et al.*, Endogenous microRNA can be broadly exploited to regulate transgene expression according to tissue, lineage and differentiation state. *Nature Biotechnology* **25**, 1457-1467 (2007).
47. K. Fuse *et al.*, Myeloid differentiation factor-88 plays a crucial role in the pathogenesis of coxsackievirus B3-induced myocarditis and influences type I interferon production. *Circulation* **112**, 2276-2285 (2005).
48. S. Pinkert *et al.*, Virus-Host Coevolution in a Persistently Coxsackievirus B3-Infected Cardiomyocyte Cell Line. *Journal of Virology* **85**, 13409-13419 (2011).
49. P. K. M. Cheung *et al.*, Specific interactions of mouse organ proteins with the 5'untranslated region of coxsackievirus B3: Potential determinants of viral tissue tropism. *Journal of Medical Virology* **77**, 414-424 (2005).
50. L. R. Zou *et al.*, A cluster of coxsackievirus A21 associated acute respiratory

illness: the evidence of efficient transmission of CVA21. *Archives of Virology* **162**, 1057-1059 (2017).

51. A. J. Ruiz, S. J. Russell, MicroRNAs and oncolytic viruses. *Current Opinion in Virology* **13**, 40-48 (2015).
52. Z. L. Ma *et al.*, MicroRNA-34a inhibits the proliferation and promotes the apoptosis of non-small cell lung cancer H1299 cell line by targeting TGF beta R2. *Tumor Biology* **36**, 2481-2490 (2015).
53. H. B. Sun, J. Tian, W. H. Xian, T. T. Xie, X. D. Yang, miR-34a Inhibits Proliferation and Invasion of Bladder Cancer Cells by Targeting Orphan Nuclear Receptor HNF4G. *Disease Markers*, (2015).
54. D. Y. Kim *et al.*, A novel miR-34a target, protein kinase D1, stimulates cancer stemness and drug resistance through GSK3/beta-catenin signaling in breast cancer. *Oncotarget* **7**, 14791-14802 (2016).
55. J. Q. Liang *et al.*, LEF1 Targeting EMT in Prostate Cancer Invasion Is Regulated by miR-34a. *Molecular Cancer Research* **13**, 681-688 (2015).
56. E. Gallardo *et al.*, miR-34a as a prognostic marker of relapse in surgically resected non-small-cell lung cancer. *Carcinogenesis* **30**, 1903-1909 (2009).
57. C. S. Song *et al.*, miR-34a sensitizes lung cancer cells to cisplatin via p53/miR-34a/MYCN axis. *Biochemical and Biophysical Research Communications* **482**, 22-27 (2017).
58. J. F. Wiggins *et al.*, Development of a Lung Cancer Therapeutic Based on the Tumor Suppressor MicroRNA-34. *Cancer Research* **70**, 5923-5930 (2010).
59. D. P. Bartel, MicroRNAs: Target Recognition and Regulatory Functions. *Cell* **136**, 215-233 (2009).
60. B. P. Lewis, C. B. Burge, D. P. Bartel, Conserved seed pairing, often flanked by adenosines, indicates that thousands of human genes are microRNA targets. *Cell* **120**, 15-20 (2005).
61. V. Agarwal, G. W. Bell, J. W. Nam, D. P. Bartel, Predicting effective microRNA target sites in mammalian mRNAs. *Elife* **4**, (2015).
62. W. L. Xu, A. San Lucas, Z. X. Wang, Y. Liu, Identifying microRNA targets in different gene regions. *Bmc Bioinformatics* **15**, (2014).
63. D. Barnes, M. Kunitomi, M. Vignuzzi, K. Saksela, R. Andino, Harnessing

endogenous miRNAs to control virus tissue tropism as a strategy for developing attenuated virus vaccines. *Cell Host & Microbe* **4**, 239-248 (2008).

64. C. L. Jopling, M. K. Yi, A. M. Lancaster, S. M. Lemon, P. Sarnow, Modulation of hepatitis C virus RNA abundance by a liver-specific microRNA. *Science* **309**, 1577-1581 (2005).
65. Z. W. Liu *et al.*, Structural and functional analysis of the 5 ' untranslated region of coxsackievirus B3 RNA: In vivo translational and infectivity studies of full-length mutants. *Virology* **265**, 206-217 (1999).
66. A. Grimson *et al.*, MicroRNA targeting specificity in mammals: Determinants beyond seed pairing. *Molecular Cell* **27**, 91-105 (2007).
67. K. K. H. Farh *et al.*, The widespread impact of mammalian microRNAs on mRNA repression and evolution. *Science* **310**, 1817-1821 (2005).
68. L. P. Lim *et al.*, Microarray analysis shows that some microRNAs downregulate large numbers of target mRNAs. *Nature* **433**, 769-773 (2005).
69. H. Hamzeiy, J. Allmer, M. Yousef, Computational Methods for MicroRNA Target Prediction. *Mirnomics: Microrna Biology and Computational Analysis* **1107**, 207-221 (2014).
70. H. C. Martin *et al.*, Imperfect centered miRNA binding sites are common and can mediate repression of target mRNAs. *Genome Biology* **15**, (2014).
71. P. A. Lodge, M. Herzum, J. Olszewski, S. A. Huber, COXSACKIEVIRUS-B-3 MYOCARDITIS - ACUTE AND CHRONIC FORMS OF THE DISEASE CAUSED BY DIFFERENT IMMUNOPATHOGENIC MECHANISMS. *American Journal of Pathology* **128**, 455-463 (1987).
72. C. Fountzilas, S. Patel, D. Mahalingam, Review: Oncolytic virotherapy, updates and future directions. *Oncotarget* **8**, 102617-102639 (2017).
73. I. Mena *et al.*, Coxsackievirus infection of the pancreas: Evaluation of receptor expression, pathogenesis, and immunopathology. *Virology* **271**, 276-288 (2000).
74. M. T. Barger, J. E. Craighead, IMMUNOMODULATION OF ENCEPHALOMYOCARDITIS VIRUS-INDUCED DISEASE IN A/J MICE. *Journal of Virology* **65**, 2676-2681 (1991).

Acknowledgments

I would like to acknowledge all people in our lab. This work was completed under the guidance of Professor Kenzaburo Tani and Drs. Shohei Miyamoto and Yasushi Soda. I would like to appreciate Dr. Yasunori Ota (Department of Pathology, Research Hospital, Institute of Medical Science) for great help in pathological examination, Ms. Ai Sugawara, Mr. Yuto Takishima, Ms. Miyako Sagara and Mr. Tomohiro Kumaki for technical assistance, Ms.Tomoko Ando (Pathology Core Laboratory, Institute of Medical Science) for pathological specimen preparation, and Ms. Michiko Ushijima for administrative assistance. I also thank Drs. Liao Jiyuan, Lisa Hirosek, Yasuki Hijikata, Kenichiro Hara and Atsufumi Iwanaga for useful suggestion and discussion. This work was supported by research funding from Shinnihonseiyaku Co., and neopharma Japan Co., Ltd.